MODELING AND MOTION SIMULATION OF AN UNDERWATER VEHICLE

A THESIS SUBMITTED TO
THE GRADUATE SCHOOL OF NATURAL AND APPLIED SCIENCES
OF
MIDDLE EAST TECHNICAL UNIVERSITY

BY

KORAY KÜÇÜK

IN PARTIAL FULFILLMENT OF THE REQUIREMENTS
FOR
THE DEGREE OF MASTER OF SCIENCE
IN
MECHANICAL ENGINEERING

SEPTEMBER 2007

MODELING AND MOTION SIMULATION OF AN UNDERWATER VEHICLE

submitted by **KORAY KÜÇÜK** in partial fulfillment of the requirements for the degree of **Master of Science in Mechanical Engineering Department, Middle East Technical University** by,

Prof. Dr. Canan Özgen _____
Dean, Graduate School of **Natural and Applied Sciences**

Prof. Dr. S. Kemal İder _____
Head of Department, **Mechanical Engineering**

Prof. Dr. M. Kemal Özgören _____
Supervisor, **Mechanical Engineering Dept., METU**

Examining Committee Members:

Prof. Dr. Reşit Soylu _____
Mechanical Engineering Dept., METU

Prof. Dr. M. Kemal Özgören _____
Mechanical Engineering Dept., METU

Prof. Dr. S. Kemal İder _____
Mechanical Engineering Dept., METU

Prof. Dr. Kemal Leblebicioğlu _____
Electric and Electrical Engineering Dept., METU

Assist. Prof. Dr. Yiğit Yazıcıoğlu _____
Mechanical Engineering Dept., METU

Date: 07.09.2007

I hereby declare that all information in this document has been obtained and presented in accordance with academic rules and ethical conduct. I also declare that, as required by these rules and conduct, I have fully cited and referenced all material and results that are not original to this work.

Name, Last Name : Koray KÜÇÜK
Signature :

ABSTRACT

MODELING AND MOTION SIMULATION OF AN UNDERWATER VEHICLE

Küçük, Koray
M.S., Department of Mechanical Engineering
Supervisor: Prof. Dr. M. Kemal Özgören

September 2007, 107 pages

This thesis involves modeling, controller design, and test case simulations for an underwater vehicle. Firstly, a complete dynamic model of the vehicle is developed with six degrees of freedom. The model includes the nonlinearities associated with the hydrodynamic forces and moments. The thrusters of the vehicle are also modeled. Then, using appropriate linearizations of the model, position and rate controllers are designed for the forward, downward, and turning motions of the vehicle. Finally, the designed controllers are tested for various maneuvers by means of simulations using the nonlinear dynamic model of the vehicle. The simulation results show that the designed controllers are quite satisfactory for the intended maneuvers.

Keywords: Underwater Vehicle, Control, Modeling, Simulation

ÖZ

SUALTI ARACININ MODELLENMESİ VE HAREKET BENZETİMİ

Küçük, Koray
Yüksek Lisans, Makina Mühendisliği Bölümü
Tez Yöneticisi: Prof. Dr. M. Kemal Özgören

Eylül 2007, 107 sayfa

Bu tez, bir sualtı aracının modellenmesini, kontrolcü tasarımını ve test benzetimlerini içermektedir. İlk olarak aracın altı serbestlik dereceli dinamik modeli geliştirilmiştir. Bu model hidrodinamik kuvvet ve momentlerin doğrusal olmayan etkilerini içermektedir. Ayrıca aracın iticileri de modellenmiştir. Daha sonra modeller doğrusallaştırılarak, ileri, aşağı ve yatay dönüş hareketleri için hız ve pozisyon kontrolcüleri geliştirilmiştir. En sonunda, geliştirilen kontrolcüler aracın doğrusal olmayan modellerini içeren benzetimler ile, farklı manevralar için test edilmiştir. Benzetim sonuçları geliştirilen kontrolcülerin belirlenen manevralar için başarılı olduğunu göstermiştir.

Anahtar Kelimeler: Sualtı Aracı, Kontrol, Modelleme, Benzetim

To all whom dedicate their lives to sea...

ACKNOWLEDGMENTS

I would like to express my sincere gratitude to Prof. Dr. M. Kemal Özgören for his supervision, patience, encouragement and guidance through out this study.

I would also like to thank to Prof. Dr. Kemal Leblebicioğlu, supervisor of the TUBITAK supported ULISAR project, for his technical mentoring and assistance.

This work has been encouraged by TÜBİTAK-SAGE. I would like to thank my colleagues Koray Dayanç, Şamil Korkmaz, Umut Durak and Fatih Geridönmez for their support and for helpful discussions we have made throughout the study.

I would also like to express thanks to Tuba Tunçel for her support, never-ending love and encouragement during all these years.

Finally, my deepest thanks go to my family who gave me the endless support and love, which made this thesis possible.

TABLE OF CONTENTS

LIST OF TABLES

LIST OF FIGURES

LIST OF SYMBOLS

$\vec{r}_O$	Position vector of the origin of $\Im_b$ with respect to $\Im_{in}$
$\vec{r}_G$	Position vector of the center of gravity with respect to $\Im_b$
$\{\vec{r}\}^{(x)}$	Column matrix representation of vector $\vec{r}$ in $\Im_x$.
$\widehat{C}^{(x,y)}$	Component transformation matrix from frame $\Im_y$ to $\Im_x$
$\bar{r}^{(x)}$	Equivalent representation of $\{\vec{r}\}^{(x)}$
$\dot{\bar{r}}^{(x)}$	First time derivative of $\bar{r}^{(x)}$
$D_x\vec{r}$	First time derivative of vector $\vec{r}$ with respect to $\Im_x$
$\vec{H}$	Angular Momentum
$\breve{I}$	Inertia dyadic
V_s	Supplied voltage to motor
i_s	Motor current

Q	Torque of thruster
T	Force of thruster
U_a	Mean velocity of propeller
$U_{0,t}$	incident water velocity w.r.t. blade
$\dot{x}, \dot{y}, \dot{z}$	Vehicle velocity component in $\Im_e$
$\dot{x}', \dot{y}', \dot{z}'$	Vehicle perturbed velocity component in $\Im_e$
u, v, w	Vehicle velocity component in $\Im_b$
u', v', w'	Vehicle velocity component in $\Im_b$
`p,q,r	Vehicle angular velocity components in $\Im_b$
$R(x)$	Radius function of the hull
g	Gravity of earth
l,d	Length and diameter of the vehicle
X,Y,Z	Force vector component in $\Im_b$
K,M,N	Moment vector component in $\Im_b$
$X_{\dot{u}}, Y_{\dot{v}}, Y_{\dot{r}}, Z_{\dot{w}}, Z_{\dot{q}}$	Added Mass coefficients
$K_{\dot{p}}, M_{\dot{w}}, M_{\dot{q}}, N_{\dot{v}}, N_{\dot{r}}$	Added Inertia coefficients

$X_{u\|u\|}, X_{qq}, X_{rr}, Y_{v\|v\|}, Y_{r\|r\|}, Z_{w\|w\|}, Z_{q\|q\|}$	Cross flow drag coefficients
$K_{p\|p\|}, M_{w\|w\|}, M_{q\|q\|}, N_{v\|v\|}, N_{r\|r\|}$	Cross flow drag coefficients
$X_{wq}, X_{vr}, Y_{ur}, Y_{wp}, Y_{pq}, Y_{uv}, Z_{uq}, Z_{vp}, Z_{rp}$	Lift force coefficients
$M_{uq}, M_{vp}, M_{rp}, M_{uw}, N_{ur}, N_{wp}, N_{pq}, N_{uv}$	Lift moment coeffients

Greek Letters

ψ	Rotation angle of $\Im_e$ around its Z axis
θ	Rotation angle of $\Im_k$ around its Y axis
ϕ	Rotation angle of $\Im_l$ around its X axis
$\vec{\omega}_{x/y}{}^{(x)}$	Angular velocity of $\Im_x$ w.r.t. $\Im_y$
ρ	Density of water
ω_m	Thruster motor angular speed

CHAPTER 1

INTRODUCTION

Unmanned Underwater Vehicles (UUVs) are the latest development of the marine research endeavor. Work in the marine environment is challenging for many reasons. Human operators are out of their natural life space and need extra precautions to survive. Moreover, due to the complications in communication, they are more restricted than for most other environments even space to some extend. This cause difficulties to control the underwater systems, and can result in loss of the system due to an inability to communicate with or locate it.

Furthermore, there are large numbers of disturbances to these systems. Significant forces such as winds, waves, currents, and hydrodynamic and hydrostatic forces affect and disrupt operations. As a result, operations tend to be complicated and time consuming. UUVs are a recent solution for achieving desired objectives in the marine environment.

A crucial element of the operations in the marine environment has been the human element itself. As is the case in such endeavors as space exploration, protecting and supporting human life increases the size, complexity, and expense of the equipment; also cause decrease in mission duration; and added risk. The benefit of the human element is its unique ability in adaptation to achieve a variety of tasks. Moreover, since it is very likely to occur of unexpected situations in this harsh environment, which require the inimitable capability of human to use intelligence and reasoning to find solutions to new problems. Even though removing humans from such operations is highly pleasing, doing so has been challenging. Automation has advanced the process of removing the human element over time, starting with the simplest tasks. Communications methods available to these vehicles provide sufficient opportunity for human participation and intervention during the course of a mission. UUVs are significantly constrained in their ability to communicate with

external operators, and are therefore highly dependent on autonomous operation. The nature of their operating environment motivates much progress in the field of control.

1.1 History

Development of UUVs has progressed in stages over the last few centuries. Like most of the technological developments, military operations provided significant motivation to develop and advance improvements in underwater operations. As in the above discussion, military effectiveness also benefits from inclusion of the human element. One typical military objective throughout history has been to deliver an effective explosive charge below the waterline of a moving target with the objective of destroying it.

The desire to achieve this level of effectiveness, but at lower cost, resulted in development of possibly the first UUV, the Whitehead torpedo [15]. It was developed by Robert Whitehead during the latter part of the 19th century and further removed the human element. In fact, once launched, there was no human element. Whitehead overcame significant technical challenges in designing a suitable propulsion and control system for his torpedo. Propulsion was provided by a variety of different engines, and control was provided by a combination of gyroscope-based heading control and depth-cell based depth control.

Current torpedoes and UUVs are improvements on Whitehead's invention. His propulsion designs were succeeded by internal combustion engines or electric drive powered by various types of batteries. His straight-running torpedo carried no sensors, other than an exploder to detonate the warhead when it sensed contact with a solid object. However follow-on torpedoes carried equipment such as wake or acoustic sensors to detect, track, and home on targets; as well as magnetic and other sensors to sense the proximity of a target and detonate the warhead at the appropriate time. Additionally, enabling a torpedo to process its sensor data to home

in on a target required the addition of computational capability, first analog, then digital. Military necessity brought a high level of autonomy and technical sophistication to underwater vehicles. Torpedoes represent one path of development towards UUVs.

Improvement came with tethers which also contained communication channels, such as wiring or optical fiber. Access to sensed data was available instantaneously, and the device could be repositioned in response to the sensed data to adaptively plan the data gathering operation and improve the usefulness of gathered data. The feedback provided by the communications link made control of the tethered device possible, and gave rise in the 1950's to remotely operated vehicles (ROV). An ROV is typically outfitted with thrusters, control surfaces, and other equipment such that a human operator can drive the ROV by remote control in the performance of its mission. This link to a human element allows ROVs to perform complex undersea missions without the actual presence of the human, eliminating the need for human requirements such as life support and protection at depth. Instead, the human element is located at a safe distance, either on a support vessel or at a networked location thousands of miles away. Additionally, the electrical connection to the surface vessel provides essentially unlimited power to the device

Versatile as ROVs are, there are still limitations to be overcome. The requirement for a tether and support vessel limits the operations of the ROV to the length of the tether, and the speed at which the tether can be towed. Additionally, the necessity of the surface vessel limits ROV operations to areas accessible to the surface vessel, something which may be constrained by sea conditions, hydrography, ice, hostile action, or the desire to remain covert. Also, there is the expense of a continuously present support vessel. UUVs represent a follow-on development in both sequences of technological progress. They build on the fusion of propulsion, control, and guidance/logic technology developed to improve torpedo capabilities, and they are used as platforms to carry the sensors that have been tethered to other vessels. In

doing so, those sensors may be employed more effectively than by tethered or other means.

1.2 UUV Limitations

UUVs, however, are by no means a panacea. For all their advantages, there are areas in which they are inferior to tethered vehicles. One consequence removing the tether is that power is limited to what can be carried onboard. This limitation was the motivation for the development of nuclear power on manned submarines, and this same limitation on smaller, unmanned UUVs that has spurred development of advanced battery and fuel cell technology. Untethered vehicles also allow little or no human involvement in their mission, due to the limited communications bandwidth available. As a result, the complexity of their missions is limited by the degree to which they can be automated.

Overcoming this limitation motivates further research in autonomy and underwater communications. A related consequence of this limited communications bandwidth is limited access by the operator to data gathered by the UUV. The most common method of retrieving the data gathered by the UUV is to recover the vehicle at the end of its mission and download the data via a computer network connection. In time-critical operations the resulting time delay may be unacceptable. Other methods, such as lowbandwidth acoustic communications or periodic radio communications periods on the surface, are also available but may not be operationally desirable. If covertness is a requirement for the operation, one reason for using an UUV instead of a vehicle tethered to a surface vessel, such methods of transmitting data may compromise covertness.

1.3 Literature Survey:

The REMUS vehicle was developed at Wood's Hole Oceanographic Institute (WHOI) in the Oceanographic Systems Laboratory. It is designed to perform hydrographic reconnaissance in the shallow water zone from 40 to 100 feet. As seen in Figure 1, it is 62 inches long and 7.5 inches in diameter. It weighs 80 pounds in air and can operate in depths up to 328 feet, but typically operates between 10 and 66 feet. The aft end thruster enables REMUS to reach a maximum speed is 5.6 knots. Its four fins, two horizontal and two vertical on either side and just forward of the thruster, allow pitch and yaw motions for maneuvering

Figure 1 The REMUS Autonomous Underwater Vehicle

Remus has been used to conduct broad range of researches especially in motion simulation and motion control fields. Chuhran [1] worked on modeling the vehicle in a planar manner in vertical plane and ignore the horizontal plane dynamics. By simply modeling forward looking sonar Chuhran tried to control motion of the

vehicle with sliding mode control and implement bearing and range weighting functions that form the gain factor for a dynamic obstacle avoidance behavior.

Prestero [3] aimed to compose a detailed simulation of REMUS vehicle including 6 degree of freedom. In scope of this work linearized depth plane controller have been developed. To compare some estimated hydrodynamic coefficients and measure the effectiveness of the designed controller that is based on the developed simulation some field experiments have been performed.

Another work by Håvard Bø [12] also focused on the estimation of the dynamics of underwater vehicles. The results of Håvard are not limited to a specific design of a vehicle. But for an example case study an autonomous underwater vehicle that is being developed under a joint Indian-Portuguese project, MAYA, was use. In order to achieve required the hydrodynamic derivatives for a body of revolution, they used empirical methods. The USAF Stability and Control Datcom which is a data reference library developed to determine the analogous aerodynamic stability derivatives for aircrafts, was used as a tool for obtaining estimates of the non-dimensional coefficients in an incompressible medium.

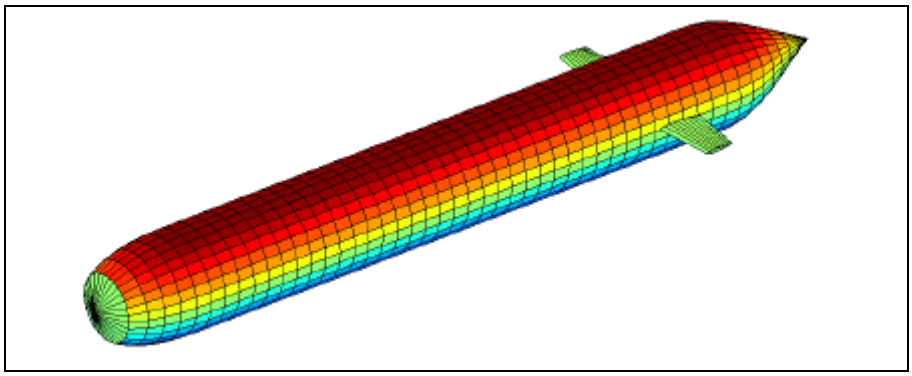

Figure 2 MAYA model used to estimate hydrodynamic coefficients

The models and hydrodynamic coefficient estimation methodologies which are stated above mostly focused on torpedo shaped slender vehicles which have one thruster and used very simple models to expressing thruster dynamics. A. J. Healey, S. M. Rock, S. Cody, D. Miles, and J. P. Brown [11] represented a novel approach in thruster modeling. The model developed by this work covers all real world phenomena including transient response through coupling of a blade, motor and fluid dynamics. The detail of this model is given in Chapter 2.

Since the design of the motion controller of an UUV is a challenging issue due to complexity of problem, it has been a preferred subject in UUV researches. Anthony J. Healey and David Lienard [10] represented a methodology that is used to decouple and linearize highly non-linear, coupled and containing uncertainties on parameters. The work used the Navy's DSRV vehicle, for case studies. The designed multivariable sliding mode autopilot based on state feedback, is composed on

- Surge Speed control

- Steering (Yaw) control
- Diving control

The results are satisfactory, designed controllers showed enough robustness in the presence of neglected degrees of freedom. Another outcome of this work is path planning algorithm that uses line of sight approach has shown that the method is robust. But in cases where tight turning maneuvers needed guidance method revealed inaccurate. In this work it is stated that *"Path planning algorithms must take vehicle dynamics into account. Ocean currents effect the ability of the LOS guidance to drive the vehicle to its desired waypoint and must be compensated by an added feed forward term in the steering controller based on a current magnitude and direction estimate."*

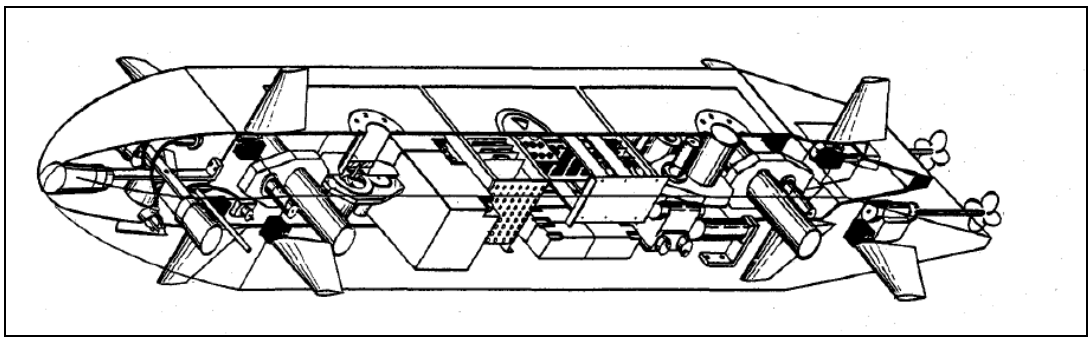

Figure 3 Navy's DSRV vehicle

1.4 Motivation and Objectives

The primary motivation of this thesis is the ULISAR (*Ulusal İnsansız Sualtı Aracı, National Unmanned Underwater Vehicle*) project supervised by Prof. Dr. Kemal Leblebicioğlu with the support of TÜBİTAK (The Scientific and Technological

Research Council of Turkey). This project aims to accomplish design, manufacture a prototype and carry out performance tests for an underwater vehicle. As one of the main research branches of the ULISAR project, the main goal of this thesis is to model such a vehicle dynamically and design a controller for some basic maneuvers such as moving forward/backward, ascending/descending, and turning. To accomplish this goal three objectives are chosen.

The first objective is to model the dynamics of the vehicle with six degrees of freedom. The model will include the nonlinear hydrodynamic effects and the thruster dynamics. It is intended to list the data requirements for these models and by use of generic empirical methods a parameter calculation tool will be developed.

The second objective is the controller design for basic maneuvers. The developed model will be linearized to design the surge, heave, pitch and turning motion controllers. Design approach for the controllers will be based on the state feedback method. The controllers will be tuned so that the output errors and the maneuvering control effort are minimized.

The third objective is to develop a simulation tool to test the effectiveness of the vehicle with the designed controllers. The simulation tool will include nonlinear dynamics of the model. This simulation module will include thruster, hydrodynamic and hydrostatic models. The intended simulation tool will be capable of simulating any underwater vehicle which is thrust controlled. This generic structure of the tool will be beneficial since it will be easy to adapt the tool to any change in the design.

CHAPTER 2

SYSTEM MODELING

In order to begin the controller design and analyze effectiveness of vehicle we need a test platform. Since the vehicle is controlled in four degrees of freedom it is essential to involve full dynamics to test the each controller responses, the effects of each controller to other dynamics, and uncontrolled dynamics to overall performance. Models have to be realistic to test our designed controllers and vehicle effectiveness.

In this chapter we define the required models which are needed to accomplish motion simulation in six degree of freedom. These models also will also be simplified in order to design controllers.

2.1 Equations of Motion

2.1.1 Reference Frames

We need to define the frames which will be used to resolve vector space representation to matrix representation. We will use two different frames

$\Im_e$: Earth surface fixed frame.

$\Im_b$: Body fixed frame.

The body-fixed coordinate system (x_b, y_b, z_b) has the origin located at the center of buoyancy of the vehicle. Since position of the center of gravity may be differ due to change in inner configuration of the vehicle, locating origin of the $\Im_b$ on buoyancy center is a widespread preference in underwater vehicle simulation applications.

The coordinate system is fixed to the underwater vehicle. The x_b-axis points forward along the body, the y_b-axis points in the direction of the starboard of the hull and the z_b-axis points the bottom of the vehicle.

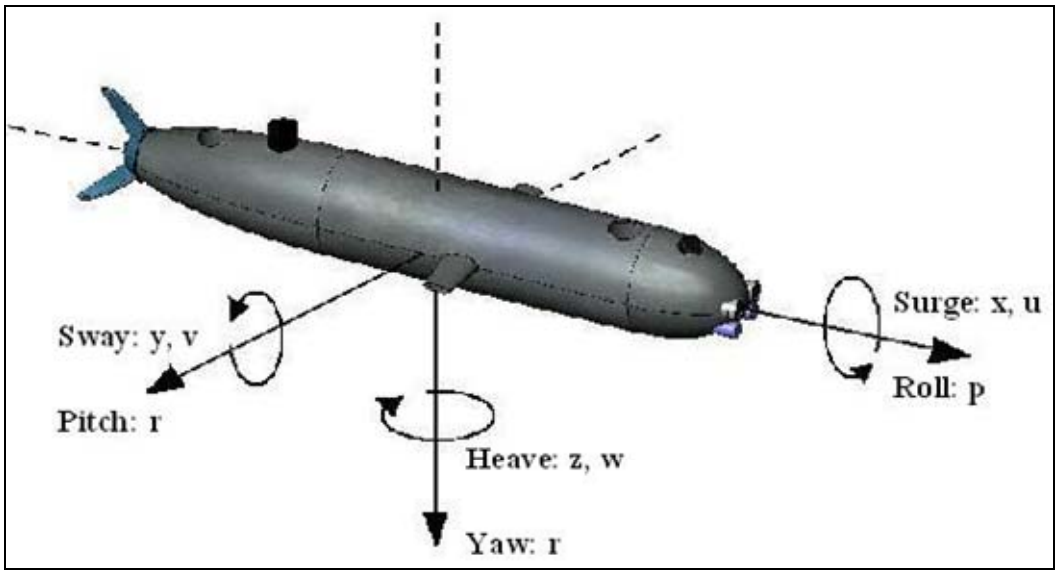

Figure 4 Body Fixed Coordinate system

In the Earth-fixed coordinate system (*x, y, z*), the *x-y* plane is normal to the local gravitational vector. In this thesis study, the vehicle is assumed to travel short distances, therefore earth is assumed to be flat and the effect of its rotational velocity is neglected. By these assumptions, the Earth-fixed coordinate system is regarded as an inertial coordinate system.

Rotated frame based transformations used to represent relative orientation of the frames with each other. One can map two frames with the given transformation order in (2.1).

$$\Im_e \xrightarrow[\psi]{\vec{u}_3^e=\vec{u}_3^k} \Im_k \xrightarrow[\theta]{\vec{u}_2^k=\vec{u}_2^l} \Im_l \xrightarrow[\phi]{\vec{u}_1^l=\vec{u}_1^b} \Im_b \tag{2.1}$$

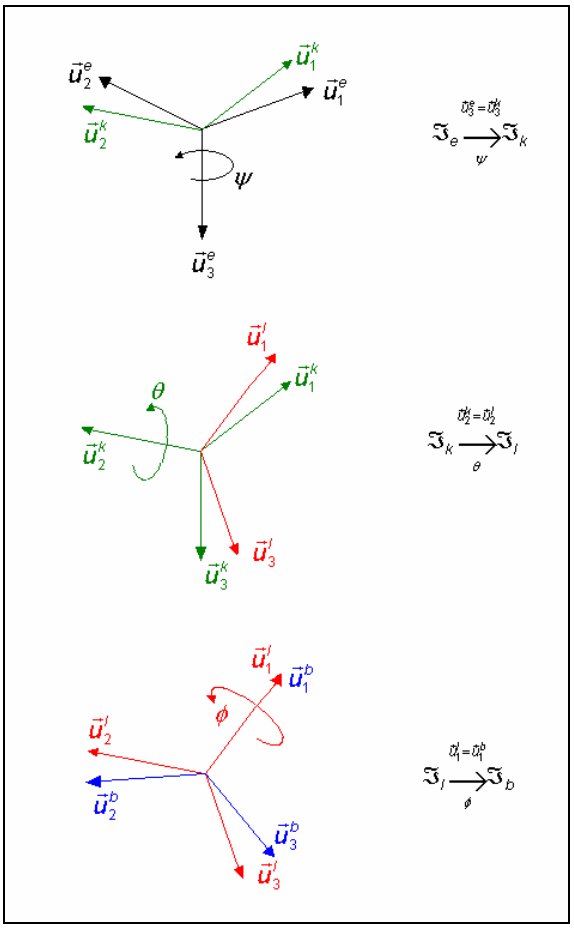

Figure 5 Rotated Frame Based Transformation

Transformations are defined by means of Euler angles. To find the transformation matrix between these frames basic rotation matrices are used. Which are given in equations (2.3), (2.4), (2.5) respectively.

$$\hat{C}^{(e,b)} = \hat{C}^{(e,k)} \times \hat{C}^{(k,l)} \times \hat{C}^{(l,b)} \tag{2.2}$$

$$\hat{C}^{(e,k)} = \begin{bmatrix} \cos\psi & -\sin\psi & 0 \\ \sin\psi & \cos\psi & 0 \\ 0 & 0 & 1 \end{bmatrix} \tag{2.3}$$

$$\hat{C}^{(k,l)} = \begin{bmatrix} \cos\theta & 0 & \sin\theta \\ 0 & 1 & 0 \\ -\sin\theta & 0 & \cos\theta \end{bmatrix} \tag{2.4}$$

$$\hat{C}^{(l,b)} = \begin{bmatrix} 1 & 0 & 0 \\ 0 & \cos\phi & -\sin\phi \\ 0 & \sin\phi & \cos\phi \end{bmatrix} \tag{2.5}$$

$$\hat{C}^{(e,b)} = \begin{bmatrix} \cos\psi\cos\theta & \cos\psi\sin\theta\sin\phi - \sin\psi\cos\phi & \cos\psi\sin\theta\cos\phi + \sin\psi\sin\phi \\ \sin\psi\cos\theta & \sin\psi\sin\theta\sin\phi + \cos\psi\cos\phi & \sin\psi\sin\theta\cos\phi - \cos\psi\sin\phi \\ -\sin\theta & \cos\theta\sin\phi & \cos\theta\cos\phi \end{bmatrix}$$

(2.6)

In order to find the earth frame velocities, body fixed velocities can be converted as;

$$\begin{bmatrix} \dot{x} & \dot{y} & \dot{z} \end{bmatrix}^T = \hat{C}^{(e,b)} \begin{bmatrix} u & v & w \end{bmatrix}^T \tag{2.7}$$

To update the transformation matrix we need to relate body angular velocities with the Euler angle rates. Both angular rate vectors represent the same rotation with different frame based unit vector. Angular velocities can be associated each other as given in the (2.8).

$$p\vec{u}_1^b + q\vec{u}_2^b + r\vec{u}_3^b = \dot{\psi}\vec{u}_3^e + \dot{\theta}\vec{u}_2^k + \dot{\phi}\vec{u}_1^l \tag{2.8}$$

Using defined basic rotation matrices and overall transformation matrix which are given in (2.4), (2.5) (2.6) we can find the related equations as;

$$\begin{bmatrix} p \\ q \\ r \end{bmatrix} = \hat{C}^{(b,e)} \times \begin{bmatrix} 0 \\ 0 \\ \dot{\psi} \end{bmatrix} + \hat{C}^{(b,k)} \times \begin{bmatrix} 0 \\ \dot{\theta} \\ 0 \end{bmatrix} + \hat{C}^{(b,l)} \times \begin{bmatrix} \dot{\phi} \\ 0 \\ 0 \end{bmatrix} \tag{2.9}$$

$$\begin{bmatrix} p \\ q \\ r \end{bmatrix} = \hat{C}^{(e,b)^{-1}} \times \begin{bmatrix} 0 \\ 0 \\ \dot{\psi} \end{bmatrix} + \hat{C}^{(l,b)^{-1}} \times \hat{C}^{(k,l)^{-1}} \times \begin{bmatrix} 0 \\ \dot{\theta} \\ 0 \end{bmatrix} + \hat{C}^{(l,b)^{-1}} \times \begin{bmatrix} \dot{\phi} \\ 0 \\ 0 \end{bmatrix} \tag{2.10}$$

$$\begin{bmatrix} p \\ q \\ r \end{bmatrix} = \begin{bmatrix} 1 & 0 & -\sin\theta \\ 0 & \cos\phi & \sin\phi\cos\theta \\ 0 & -\sin\phi & \cos\phi\cos\theta \end{bmatrix} \begin{bmatrix} \dot{\phi} \\ \dot{\theta} \\ \dot{\psi} \end{bmatrix} \tag{2.11}$$

$$\dot{\psi} = \frac{q\sin\phi + r\cos\phi}{\cos\theta} \tag{2.12}$$

$$\dot{\theta} = q\cos\phi - r\sin\phi \tag{2.13}$$

$$\dot{\phi} = p + \left(q\sin\phi + r\cos\phi\right)\tan\theta \tag{2.14}$$

2.1.2 Translational Equation of Motion in Vector Form

To represent our dynamic equations we choose to resolve our vectors in the body frame since it is easer to represent forces and moments.

Newton's 2'nd law is valid in an inertial frame. However it is not practical to use an inertial frame since human cognition is virtually limited to perceive motion of objects with respect to Earth. In addition as stated above overall motion of the vehicle is limited in short ranges, for that reason we will neglect the motion of the earth with respect to inertial frame and take an earth fixed frame as an inertial frame.

The position of the center of gravity with respect to the selected earth fixed frame can be represented as the sum of two vectors;

$$\vec{r}_C = \vec{r}_G + \vec{r}_O \tag{2.15}$$

Newton's second law states that;

$$\sum \vec{F} = mD_e{}^2\vec{r}_C \tag{2.16}$$

Using the sum of vectors given in (2.15) we can represent the velocity vector of the center of gravity as;

$$D_e\vec{r}_C = D_e\vec{r}_G + D_e\vec{r}_O \tag{2.17}$$

After applying the transport theorem [14] and under the rigid body assumption ($D_b\vec{r}_G = 0$)

$$D_e\vec{r}_C = D_e\vec{r}_O + \vec{\omega}_{b/e} \times \vec{r}_G \tag{2.18}$$

Denoting $D_e\vec{r}_O$ as $\vec{v}_O$ and $D_e\vec{r}_C$ as $\vec{v}_C$ and differentiating both sides result in;

$$D_e\vec{v}_C = D_e\vec{v}_O + D_e\left(\vec{\omega}_{b/e} \times \vec{r}_G\right) \tag{2.19}$$

Since we try to resolve the equation of motion in the body fixed frame, we apply transport theorem again;

$$D_e\vec{v}_C = D_b\vec{v}_O + \vec{\omega}_{b/e} \times \vec{v}_O + D_b\vec{\omega}_{b/e} \times \vec{r}_G + \vec{\omega}_{b/e} \times \left(\vec{\omega}_{b/e} \times \vec{r}_G\right) \tag{2.20}$$

Returning to (2.16) gives the resultant vector representation of the translational equation as;

$$\sum \vec{F} = m\left(D_b\vec{v}_O + \vec{\omega}_{b/e} \times \vec{v}_O + D_b\vec{\omega}_{b/e} \times \vec{r}_G + \vec{\omega}_{b/e} \times \left(\vec{\omega}_{b/e} \times \vec{r}_G\right)\right) \tag{2.21}$$

The more detailed version of this derivation can be found in [13]

2.1.3 Attitude Equation of Motion in Vector Form

To find the attitude equation of motion Euler's equation is used which is expressed in an inertial frame similar to the Newton's 2nd law as

$$\sum \vec{M} = D_e \vec{H} \tag{2.22}$$

$$\vec{H} = \breve{I} \cdot \vec{\omega}_{b/e} \tag{2.23}$$

Using the definition of angular momentum of a rigid body (2.23) we can obtain equation of motion in vector form [13];

$$\sum \vec{M} = \breve{I} \cdot D_b \vec{\omega}_{b/e} + \vec{\omega}_{b/e} \times \left(\breve{I} \cdot \vec{\omega}_{b/e} \right) + m\vec{r}_G \times \left(\vec{v}_O + \vec{\omega}_{b/e} \times \vec{v}_O \right) \tag{2.24}$$

2.1.4 Equations of Motion in Component Form

The vector forms of the equations of motion can be decomposed into components defined in $\Im_b$ as given below;

$$m\left[\dot{u} - vr + wq - x_G \left(q^2 + r^2 \right) + y_G \left(pq - \dot{r} \right) + z_G \left(pr + \dot{q} \right) \right] = \sum X \tag{2.25}$$

$$m\left[\dot{v} + ur - wp + x_G \left(pq + \dot{r} \right) - y_G \left(p^2 + r^2 \right) + z_G \left(qr - \dot{p} \right) \right] = \sum Y \tag{2.26}$$

$$m\left[\dot{w} - uq + vp + x_G \left(pr - \dot{q} \right) + y_G \left(qr + \dot{p} \right) - z_G \left(p^2 + q^2 \right) \right] = \sum Z \tag{2.27}$$

$$\begin{aligned} &I_{xx}\dot{p} + \left(I_{zz} - I_{yy} \right) qr + I_{xy} \left(pr - \dot{q} \right) - I_{yz} \left(q^2 - r^2 \right) - I_{xz} \left(pq + \dot{r} \right) \cdots \\ &+ m\left[y_G \left(\dot{w} - uq + vp \right) - z_G \left(\dot{v} + ur - wp \right) \right] = \sum K \end{aligned} \tag{2.28}$$

$$I_{yy}\dot{q}+\left(I_{xx}-I_{zz}\right)pr-I_{xy}\left(qr+\dot{p}\right)+I_{yz}\left(pq-\dot{r}\right)+I_{xz}\left(p^2-r^2\right)\cdots \\ -m\left[x_G\left(\dot{w}-uq+vp\right)-z_G\left(\dot{u}-vr+wq\right)\right]=\sum M \tag{2.29}$$

$$I_{zz}\dot{r}+\left(I_{yy}-I_{xx}\right)pq-I_{xy}\left(p^2-q^2\right)-I_{yz}\left(pr+\dot{q}\right)+I_{xz}\left(qr-\dot{p}\right)\cdots \\ +m\left[x_G\left(\dot{v}+ur-wp\right)-y_G\left(\dot{u}-vr+wq\right)\right]=\sum N \tag{2.30}$$

2.2 Forces and Moments

Forces and moments are formed due to the gravitational field of the earth, hydrostatic effects, hydrodynamic effects and thrusters. Models are presented below to calculate these forces.

2.2.1 Hydrostatic Model

Under the effect of the earth gravitational field, the vehicle experiences some force distribution. Moreover due to the weight of the water, pressure distribution occurs all over the hull of the vehicle. These force fields can be combined into resultant force vectors denoted as weight and buoyancy. The weight vector in the earth frame can be shown as;

$$\left\{\vec{F}_W\right\}^{(e)}=\begin{bmatrix}0\\0\\mg\end{bmatrix}=\begin{bmatrix}0\\0\\W\end{bmatrix} \tag{2.31}$$

Where m is the mass of the vehicle and g is local gravitational acceleration. The buoyancy of the vehicle in the earth frame can be represented as;

$$\left\{\vec{F}_B\right\}^{(e)}=\begin{bmatrix}0\\0\\-\rho\nabla g\end{bmatrix}=\begin{bmatrix}0\\0\\-B\end{bmatrix} \tag{2.32}$$

Where ρ represents the water density and ∇ is the total volume of the vehicle.

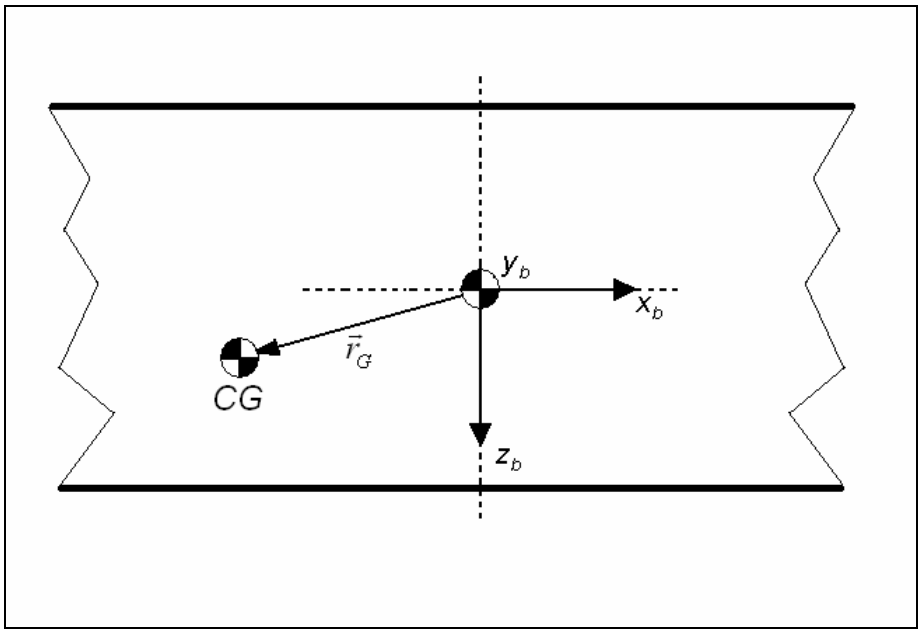

Figure 6 Position of C.G. in $\Im_b$

Since the application point of the weight vector does not coincide with the origin of the body frame, effective force vector induces a restoring moment. This moment can be found as;

$$\vec{M}_W = \vec{r}_G \times \vec{F}_W \tag{2.33}$$

Since the resolution frame for the equations of motion is the body fixed frame, it is necessary to resolve these forces and moments in that frame. So using the inverse of transformation matrix given in (2.6) force transformation can be expressed as;

$$\left\{\vec{F}_{HS}\right\}^{(b)} = \hat{C}^{(b,e)} \times \left\{\vec{F}_W\right\}^{(e)} + \hat{C}^{(b,e)} \times \left\{\vec{F}_B\right\}^{(e)} \tag{2.34}$$

Similarly moment equation can be represented as;

$$\left\{\vec{M}_W\right\}^{(b)} = \left\{\vec{r}_G\right\}^{(b)} \times \left(\hat{C}^{(e,b)^{-1}} \times \left\{\vec{F}_W\right\}^{(b)}\right) \tag{2.35}$$

Making appropriate matrix operations and using the inverse of transformation matrix given in (2.36) components of the hydrostatic forces and the moment can be found as:

$$\hat{C}^{(b,e)} = \hat{C}^{(e,b)^{-1}} = \begin{bmatrix} \cos\psi\cos\theta & \sin\psi\cos\theta & -\sin\theta \\ \cos\psi\sin\theta\sin\phi - \sin\psi\cos\phi & \sin\psi\sin\theta\sin\phi + \cos\psi\cos\phi & \cos\theta\sin\phi \\ \cos\psi\sin\theta\cos\phi + \sin\psi\sin\phi & \sin\psi\sin\theta\cos\phi - \cos\psi\sin\phi & \cos\theta\cos\phi \end{bmatrix} \tag{2.36}$$

$$X_{HS} = \left(B - W\right)\sin\theta \tag{2.37}$$

$$Y_{HS} = \left(W - B\right)\cos\theta\sin\phi \tag{2.38}$$

$$Z_{HS} = \left(W - B\right)\cos\theta\cos\phi \tag{2.39}$$

$$K_{HS} = -W\cos\theta\left(z_G\sin\phi + y_G\cos\phi\right) \tag{2.40}$$

$$M_{HS} = -W\left(z_G\sin\theta + x_G\cos\theta\cos\phi\right) \tag{2.41}$$

$$N_{HS} = -W\left(x_G\cos\theta\sin\phi + y_G\sin\theta\right) \tag{2.42}$$

2.2.2 Hydrodynamic Model

Since the scope of this thesis concentrates on the dynamic modeling and control approaches, the hydrodynamic model is directly implanted from [3]. Prestero conducted a series of experiments and validates the hydrodynamic coefficients for REMUS vehicle which has a similar outer configuration to the vehicle that is investigated in this thesis.

Here we will state the components which are representing the body/fluid contradictions. Afterwards, the estimation methods to find these coefficients will be given. The vehicle parameters needed by the model coefficient derivations are given in Chapter 4 in details.

2.2.2.1 Added Mass and Inertia

Added mass and inertia used to represent the phenomena occurs by the pressure induced forces and the moments due to a forced harmonic motion of the body. The vehicle motion will force the whole fluid to oscillate with different fluid particle amplitudes in phase with the forced harmonic motion of the vehicle. Amplitudes will decay far away from the surface of the vehicle. These forces and moments are proportional to the acceleration of the body.

For general case the added inertia matrix is defined as:

$$M_A = -\begin{bmatrix} X_{\dot{u}} & X_{\dot{v}} & X_{\dot{w}} & X_{\dot{p}} & X_{\dot{q}} & X_{\dot{r}} \\ Y_{\dot{u}} & Y_{\dot{v}} & Y_{\dot{w}} & Y_{\dot{p}} & Y_{\dot{q}} & Y_{\dot{r}} \\ Z_{\dot{u}} & Z_{\dot{v}} & Z_{\dot{w}} & Z_{\dot{p}} & Z_{\dot{q}} & Z_{\dot{r}} \\ K_{\dot{u}} & K_{\dot{v}} & K_{\dot{w}} & K_{\dot{p}} & K_{\dot{q}} & K_{\dot{r}} \\ M_{\dot{u}} & M_{\dot{v}} & M_{\dot{w}} & M_{\dot{p}} & M_{\dot{q}} & M_{\dot{r}} \\ N_{\dot{u}} & N_{\dot{v}} & N_{\dot{w}} & N_{\dot{p}} & N_{\dot{q}} & N_{\dot{r}} \end{bmatrix} \tag{2.43}$$

Due to body top-bottom and port-starboard symmetry, the vehicle added mass matrix reduces to:

$$M_A = -\begin{bmatrix} X_{\dot{u}} & 0 & 0 & 0 & 0 & 0 \\ 0 & Y_{\dot{v}} & 0 & 0 & 0 & Y_{\dot{r}} \\ 0 & 0 & Z_{\dot{w}} & 0 & Z_{\dot{q}} & 0 \\ 0 & 0 & 0 & K_{\dot{p}} & 0 & 0 \\ 0 & 0 & M_{\dot{w}} & 0 & M_{\dot{q}} & 0 \\ 0 & N_{\dot{v}} & 0 & 0 & 0 & N_{\dot{r}} \end{bmatrix} \tag{2.44}$$

Axial Added Mass:

To estimate the axial added mass term, vehicle hull shape is approximated by a similitude ellipsoid which has the major axis length as the half of the vehicle length, and the minor axis length equal to the half of the vehicle diameter. In [21] Blevins gives the following empirical formula for the axial added mass of an ellipsoid:

$$X_{\dot{u}} = -\frac{4\alpha\rho\pi}{3}\left(\frac{l}{2}\right)\left(\frac{d}{2}\right)^2 \tag{2.45}$$

Empirical parameter α is measured by Blevins and given in Table 1:

Table 1 Axial Added Mass Empirical Parameter α

l/d	α
0.1	6.148
0.2	3.008
0.4	1.428
0.6	0.9078
0.8	0.6514
1.0	0.5000
1.5	0.3038
2.0	0.2100
2.5	0.1563
3.0	0.1220
5.0	0.05912
7.0	0.03585
10.0	0.02071

Strip Theory:

For slender bodies an estimate of the hydrodynamic derivatives can be obtained by applying the strip theory. The principle of strip theory involves dividing the

submerged part of the vehicle into a number of strips. Then two dimensional theoretical hydrodynamic coefficients of each strip are calculated. Later on, calculated two dimensional coefficients of each strip are integrated all over the hull surface to find three dimensional terms.

Some useful two dimensional added mass terms are given below. Newman [16] states that the added mass per unit length of a single cylindrical strip is given as:

$$m_a(x) = \pi\rho R(x)^2 \tag{2.46}$$

The added mass of a circle with fins is given in Blevins as:

$$m_{a,f}(x) = \pi\rho\left(a_{fin}{}^2 - R(x)^2 \frac{R(x)^4}{a_{fin}{}^2} \right) \tag{2.47}$$

Cross flow Added Mass:

The given theoretical equations integrated along hull with the related sections result in:

$$Y_{\dot{v}} = -\int_{x_t}^{x_f} m_a(x)\,dx - \int_{x_f}^{x_{f2}} m_{af}(x)\,dx - \int_{x_{f2}}^{x_{b2}} m_a(x)\,dx \tag{2.48}$$

$$M_{\dot{w}} = \int_{x_t}^{x_f} x m_a(x)\,dx - \int_{x_f}^{x_{f2}} x m_{af}(x)\,dx - \int_{x_{f2}}^{x_{b2}} x m_a(x)\,dx \tag{2.49}$$

$$M_{\dot{q}} = -\int_{x_t}^{x_f} x^2 m_a(x)\,dx - \int_{x_f}^{x_{f2}} x^2 m_{af}(x)\,dx - \int_{x_{f2}}^{x_{b2}} x^2 m_a(x)\,dx \tag{2.50}$$

Due to the longitudinal symmetry other added mass terms can be found as:

$$Z_{\dot{w}} = Y_{\dot{v}}, \qquad N_{\dot{v}} = Y_{\dot{r}} = -Z_{\dot{q}} = -M_w \tag{2.51}$$

Rolling Added Mass:

Theoretical calculations in literature are not intended to adjoin effects of the surface impurities of the hull. For axis symmetric body cross sections theoretical values for rolling added mass is zero. Furthermore these models are deficient in interpretation of the roll added mass for circle with fins. Therefore to estimate the rolling added mass, we will assume that, the smooth sections of the vehicle hull do not generate any added mass in roll. We will also neglect the added mass generated by the other asymmetric body parts like the port and the starboard thrusters. Under those assumptions, the section containing stabilization fins is the only portion of the body that rolling added mass contribution is calculated.

Blevins gives the following empirical formula for the added mass of a rolling circle with fins:

$$K_{\dot{p}} = -\int_{x_f}^{x_{f2}} \frac{2}{\pi} \rho a^4 dx \tag{2.52}$$

Added Mass Cross Terms:

As a result of added mass couplings some cross terms are formed. These parameters can be found using calculated coefficients:

$$X_{wq} = Z_{\dot{w}} \qquad X_{qq} = Z_{\dot{q}} \qquad X_{vr} = -Y_{\dot{v}} \qquad X_{rr} = -Y_{\dot{r}}$$
$$Y_{ur} = -X_{\dot{u}} \qquad Y_{wp} = -Z_{\dot{w}} \qquad Y_{pq} = -Z_{\dot{q}}$$
$$Z_{uq} = -X_{\dot{u}} \qquad Z_{vp} = Y_{\dot{v}} \qquad Z_{rp} = Y_{\dot{r}}$$
$$M_{uwa} = -\left(Z_{\dot{w}} - X_{\dot{u}}\right) \qquad M_{vp} = -Y_{\dot{r}} \qquad M_{rp} = \left(K_{\dot{p}} - N_{\dot{r}}\right) \qquad M_{uq} = -Z_{\dot{q}}$$
$$N_{uva} = -\left(X_{\dot{u}} - Y_{\dot{v}}\right) \qquad N_{wp} = Z_{\dot{q}} \qquad N_{pq} = -\left(K_{\dot{p}} - M_{\dot{q}}\right) \qquad N_{ur} = Y_{\dot{r}}$$

2.2.2.2 Drag Force

Axial Drag:

In a viscous fluid, frictional forces exist. These frictional forces can be defined as;

$$X = -\frac{1}{2}\rho C_D A_f u|u| \tag{2.53}$$

So for steady velocities and no change in velocity in vehicle we can simply donate the coefficient as;

$$X_{u|u|} = -\frac{1}{2}\rho C_D A_f \tag{2.54}$$

To approximate the C_D the empirical formulae is given in [3] is:

$$C_D = \frac{c_{ss}\pi A_p}{A_f}\left[1 + 60\left(\frac{d}{l}\right)^3 + 0.0025\left(\frac{l}{d}\right)\right] \tag{2.55}$$

Where c_{ss} is Schoenherr's value for flat plate skin friction, it is stated that c_{ss} can be estimated as $3.397 \times 10{-}3$ [3]. For REMUS vehicle corresponding C_D turns out to be in the range of 0.11 and 0.13. However after conducting some experiments C_D appears to be 0.27. So we take the experimental value for our further calculations.

Cross flow Drag:

Vehicle cross flow drag is superimposed in to two effects by means of hull and fin drag forces. The method used for calculating the vehicle drag is analogous to strip theory, which is the method used to calculate the vehicle added inertia terms. The total vehicle drag is calculated by means of integration of the drag coefficients belongs to two-dimensional cylindrical vehicle cross-sections, overall surface.

The cross flow drag coefficients are expressed as follows:

$$Y_{v|v|} = Z_{w|w|} = -\frac{1}{2}\rho C_{Dc}\int_{x_t}^{x_{b2}} 2R(x)\,dx - 3\left(\frac{1}{2}\rho S_{fin} C_{Df}\right) \tag{2.56}$$

$$M_{w|w|} = -N_{v|v|} = \frac{1}{2}\rho C_{Dc}\int_{x_t}^{x_{b2}} 2xR(x)\,dx - 3x_{fin}\left(\frac{1}{2}\rho S_{fin} C_{Df}\right) \tag{2.57}$$

$$Y_{r|r|} = -Z_{q|q|} = -\frac{1}{2}\rho C_{Dc}\int_{x_t}^{x_{b2}} 2x|x|\,R(x)\,dx - 3x_{fin}\left|x_{fin}\right|\left(\frac{1}{2}\rho S_{fin} C_{Df}\right) \tag{2.58}$$

$$M_{q|q|} = N_{r|r|} = -\frac{1}{2}\rho C_{Dc}\int_{x_t}^{x_{b2}} 2x^3 R(x)\,dx - 3x_{fin}{}^3\left(\frac{1}{2}\rho S_{fin} C_{Df}\right) \tag{2.59}$$

The cross flow drag coefficient of a cylinder 'C_{Dc}' is estimated as 1.1. The cross flow drag coefficient for the fins (C_{Df}) is derived using the formula [3]

$$C_{Df} = 0.1 + 0.7t \tag{2.60}$$

Rolling Drag:

For added roll inertia terms we include only the effects of fins. To the same extent in roll drag we will estimate the rolling resistance of the vehicle by only assuming the principle component comes from the cross flow drag of the fins.

$$F = \left(Y_{vvf} r_{mean}\right) r_{mean}{}^2 p|p| \tag{2.61}$$

Where Y_{vvf} is the cross flow drag term of fins can be found as:

$$Y_{vvf} = -3\left(\frac{1}{2}\rho S_{fin} C_{Df}\right) \tag{2.62}$$

So the rolling drag term can be represented as:

$$K_{p|p|} = Y_{vvf} r_{mean}{}^3 \tag{2.63}$$

2.2.2.3 Lift Force and Moments

Lift force and moments results when the vehicle moving through the water at an angle of attack. These relative motion triggers flow separation, rise of the dynamical pressure below the vehicle and subsequent drop in static pressure along the upper section of the vehicle hull. This pressure difference along the hull surface is lumped into a resultant force applied at the center of pressure. As the center of pressure does not coincide with the origin of the body-fixed coordinate system, this force also leads to a pitching moment about the origin.

Body Lift Force:

The empirical formula for estimating body lift is given as:

$$L_{body} = -\frac{1}{2}\rho d^2 c_{yd} u^2 \tag{2.64}$$

Body lift coefficient which is function of angle of attack of the vehicle is expressed as:

$$c_{yd} = c_{yd}(\beta) = \frac{dc_{yd}}{d\beta}\beta \tag{2.65}$$

Angle of attack of the vehicle can be found directly by using trigonometric relation:

$$\tan\beta = \frac{w}{u} \tag{2.66}$$

For small angle of attacks it can be written as:

$$\beta \cong \frac{w}{u} \tag{2.67}$$

The lift slope is approximated as:

$$\frac{dc_{yd}}{d\beta} = c_{yd\beta} = \left(\frac{l}{d}\right) c_{y\beta} \tag{2.68}$$

For length diameter ratio in the region $6.7 \le l/d \le 10$, $c_{y\beta}$ is given as 0.1719. Substituting equations (2.65)and (2.67) into (2.64) results in:

$$L_{body} = \underbrace{-\frac{1}{2}\rho d^2 c_{yd\beta}}_{Z_{uwl}} uw \tag{2.69}$$

The body lift coefficient can be shown as:

$$Z_{uwl} = -\frac{1}{2}\rho d^2 c_{yd\beta} \tag{2.70}$$

Body Lift Moment:

For a body of revolution which undergoes a relative fluid flow with an angle of attack presence, the viscous force is assumed centered at a point between 0.6 and 0.7 of the total body length from the nose [12]. The experimental findings suggest that the flow goes smoothly around the forward end of the hull, and that the lateral force only develops on the leeward side of the rear half of the hull.

Following these findings, we will assume that, in body-fixed coordinates center of pressure is located with respect to origin:

$$x_{cp} = 0.65l - x_{CB} \tag{2.71}$$

So it is easy to show that moment coefficient can be represented as;

$$M_{uwl} = -\frac{1}{2}\rho d^2 c_{yd\beta} x_{cp} \tag{2.72}$$

Fin Lift:

The empirical formula for fin lift can be given as:

$$L_{fin} = \frac{1}{2}\rho C_L S_{fin} \alpha v_e^{\,2} \tag{2.73}$$

Fin lift coefficient C_L is a function of the effective fin angle of attack (α). The following is the empirical formula for fin lift as a function of α:

$$C_{L\alpha} = \frac{dC_L}{d\alpha} = \left[\frac{1}{2\bar{\alpha}\pi} + \frac{1}{\pi AR_e}\right]^{-1} \tag{2.74}$$

Where the factor $\bar{\alpha}$ was given in [3] as 0.9, and the effective fin aspect ratio (AR_e) is given by the formula:

$$AR_e = 2AR = 2\left(\frac{b_{fin}^{\,2}}{S_{fin}}\right) \tag{2.75}$$

Since fins are located with some offset from the origin of the body fixed coordinate system the effective velocities have to be calculated considering translational velocity effects of angular velocities. After simplifications fin lift coefficients can be found as:

$$Y_{uvf} = -\rho C_{L\alpha} S_{fin} \tag{2.76}$$

$$Z_{uwf} = Y_{uvf} \tag{2.77}$$

$$Y_{urf} = -\rho C_{L\alpha} S_{fin} x_{fin} \tag{2.78}$$

$$M_{uwf} = \rho C_{L\alpha} S_{fin} x_{fin} \tag{2.79}$$

$$N_{uvf} = -M_{uwf} \tag{2.80}$$

$$N_{urf} = -\rho C_{L\alpha} S_{fin} x_{fin}^{\ 2} \tag{2.81}$$

Parameter Combination:

Terms which are used to calculate same force or moment term can be combined as:

$$\begin{aligned}
Y_{uv} &= Y_{uvl} + Y_{uvf} \\
Y_{ur} &= Y_{ura} + Y_{urf} \\
Z_{uw} &= Z_{uwl} + Z_{uw} \\
Z_{uq} &= Z_{uqa} + Z_{uqf} \\
M_{uw} &= M_{uwa} + M_{uwl} + M_{uwf} \\
M_{uq} &= M_{uqa} + M_{uqf} \\
N_{uv} &= N_{uva} + N_{uvl} + N_{uvf} \\
N_{ur} &= N_{ura} + N_{urf}
\end{aligned} \tag{2.82}$$

2.2.3 Thruster Model

As the movement and control of vehicle are achieved by means of four thrusters, model represent the dynamic behavior of the thruster have to be appropriate in fidelity. From literature model developed by Healey [11] is found to be the proper candidate to fulfill our requirements.

In general view, model can be decomposed into three sub models. One can see these models and their data interfaces from Figure 7.

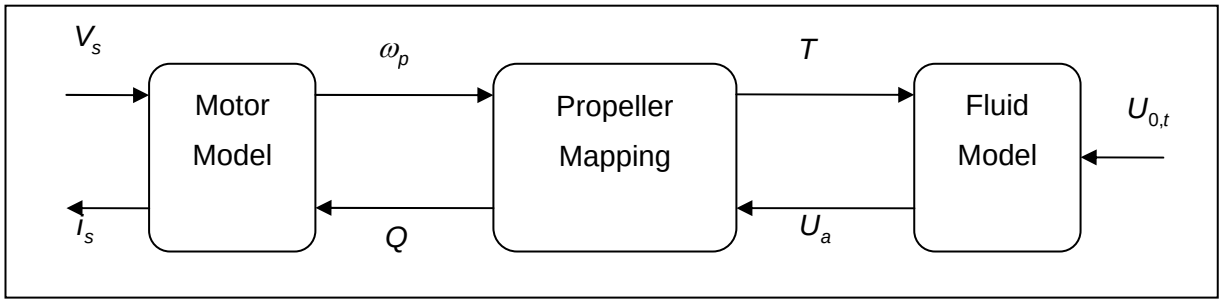

Figure 7 General view of the thruster model

2.2.3.1 Motor Model

The motor model is standard in electromechanical modeling and is based here on a dc servo-motor permanent magnet type.

$$\dot{\omega}_m = -K_1\omega_m + K_2V_s - K_hQ \tag{2.83}$$

The parameter K_h relates to the motor deceleration from propeller hydrodynamic torque loading. The total rotational inertia includes all mechanical inertia including motor, gears and propeller K_1 contains all viscous friction components as well as the motor characteristic resistance that gives effective damping to the motor response. If there is any gear reduction in the thruster actual rotation rate can be found by dividing the motor output angular rate to gear reduction ratio.

$$\omega_p = \frac{\omega_m}{N} \tag{2.84}$$

2.2.3.2 Propeller Mapping

Tangential speed of the blade is measured at some convenient radial position (usually taken at $0.7R_p$), is such that the tangential velocity of the fluid relative to the blade is given by

$$U_p = 0.7R_p \frac{\omega_m}{N} \tag{2.85}$$

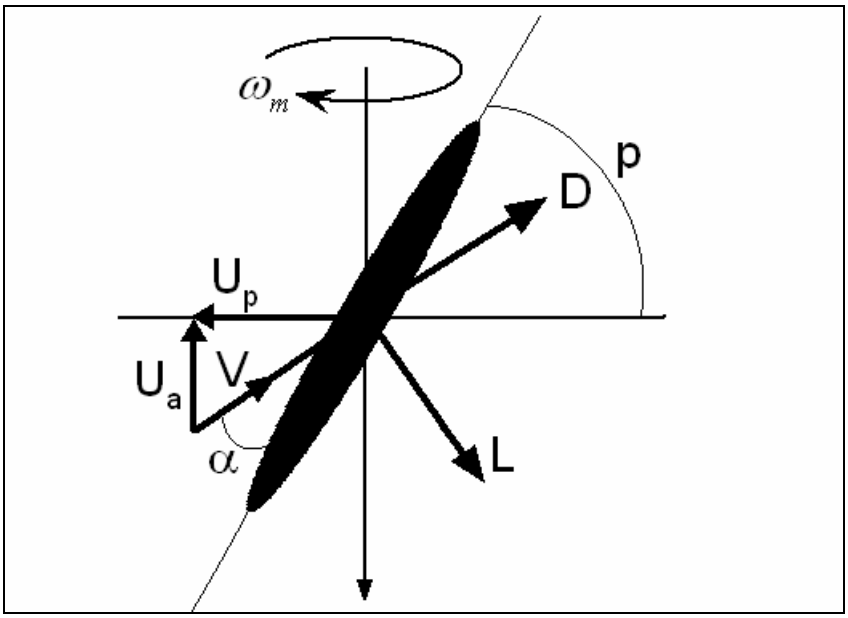

Figure 8 Top view of blade

As it can be seen from Figure 8 due to incoming fluid particles relative to the propeller blade an inlet effective angle of attack is formed. This angle of attack can be found as;

$$\alpha_e = \left(\frac{\pi}{2} - p\right) - \arctan\left(\frac{U_a}{U_p}\right) \tag{2.86}$$

The magnitude of the incoming particles with respect to blade surface can be found as;

$$V^2 = U_p{}^2 + U_a{}^2 \tag{2.87}$$

The drag and lift coefficients of the blade is assumed to be harmonic as given in the Figure 9 which is taken from [11].

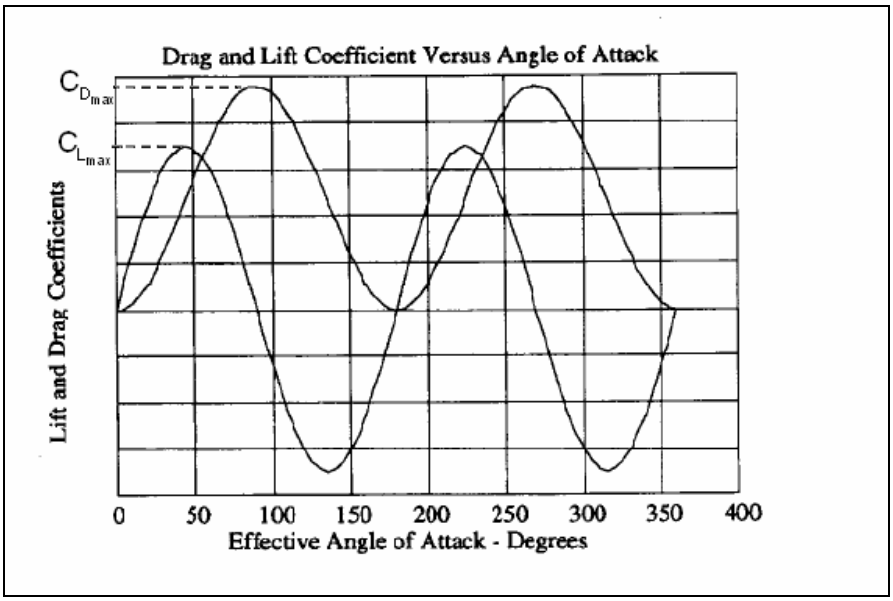

Figure 9 Lift and drag coefficients versus α_e

Using these harmonic coefficients the resultant lift and drag forces can be found as;

$$F_{lift} = \frac{1}{2}\rho V^2 A C_{L_{\max}} \sin\left(2\alpha_e\right) \tag{2.88}$$

$$F_{drag} = \frac{1}{2}\rho V^2 A C_{D_{\max}} \left(1 - \cos\left(2\alpha_e\right)\right) \tag{2.89}$$

Using these forces the thrust force and torque can be found as;

$$T = F_{lift}\cos\left(\theta\right) - F_{drag}\sin\left(\theta\right) \tag{2.90}$$

$$Q = 0.7R\left[F_{lift}\sin\left(\theta\right) + F_{drag}\cos\left(\theta\right)\right] \tag{2.91}$$

Where θ is defined as;

$$\theta = p - \alpha_e \tag{2.92}$$

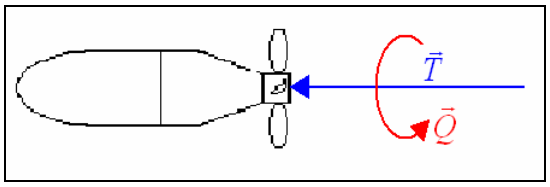

Figure 10 Torque and Force of Thruster

2.2.3.3 Fluid Model

When the angular rate of the propeller changed there will be lags in the development of changes in the axial component due to the surrounding fluids dynamics. And also during the thruster unit is advanced through the surrounding water, some effect on the inlet flow to the blades occurs. This part of the model represents the fluid dynamics.

We apply the momentum equation to a control volume surrounding the inlet flow.

$$T = (\rho AL\gamma)\dot{U}_a + (\rho A\Delta\beta)\overline{U_a}\left|\overline{U_a}\right| \tag{2.93}$$

Rearranging terms gives us;

$$\dot{U}_a = -K_4 K_3^{-1}\overline{U_a}\left|\overline{U_a}\right| + K_3^{-1}T \tag{2.94}$$

$$K_3 = \rho AL\gamma, \qquad K_4 = \rho A\Delta\beta \tag{2.95}$$

Where $\overline{U_a}$ is defined as,

$$\overline{U_a} = \left(U_a - U_{0,t}\right) \tag{2.96}$$

2.2.3.4 Implementation of Motor Model

Thruster model needs inputs from other simulation entities. These inputs are supplied voltage (V_s) and forward velocity relative to water ($U_{0,t}$). Applied voltage is output of the thruster controller. Relative forward velocity is calculated for each thruster is as given below.

To begin with relative velocity of vehicle is calculated by adding current velocity on the vehicle velocity in body fixed frame. Since the current velocity is defined in the earth fixed frame we have transform it to body fixed frame:

$$\left\{\vec{V}_{rel}\right\}^{(b)} = \left\{\vec{V}_O\right\}^{(b)} + \hat{C}^{(b,e)}\left\{\vec{V}_{cur}\right\}^{(e)} \tag{2.97}$$

Than for each motor forward velocity effects of angular rates of vehicle is calculated and added on relative velocity as:

$$\left\{\vec{V}_0\right\}^{(b)} = \left\{\vec{V}_{rel}\right\}^{(b)} + \left\{\vec{\omega}_{b/e}\right\}^{(b)} \times \left\{\vec{r}_t\right\}^{(b)} \tag{2.98}$$

Then,

- for starboard and port thrusters first element of $\left\{\vec{V}_0\right\}^{(b)}$
- for front and back thrusters third element of $\left\{\vec{V}_0\right\}^{(b)}$

are taken to find the relative forward speed of the thrusters.

To find the resultant thrust force and moments applied on vehicle in body fixed frame:

$$\begin{bmatrix} \left\{\vec{F}_T\right\}^{(b)} \\ \left\{\vec{M}_T\right\}^{(b)} \end{bmatrix} = \begin{bmatrix} X_T \\ Y_T \\ Z_T \\ K_T \\ M_T \\ N_T \end{bmatrix} = \begin{bmatrix} T_{pt} + T_{st} \\ 0 \\ T_{ft} + T_{bt} \\ Q_{pt} + Q_{ft} \\ T_{bt} r_{bt,1} - T_{ft} r_{ft,1} \\ T_{pt} r_{pt,2} - T_{st} r_{st,2} + Q_{ft} + Q_{bt} \end{bmatrix} \tag{2.99}$$

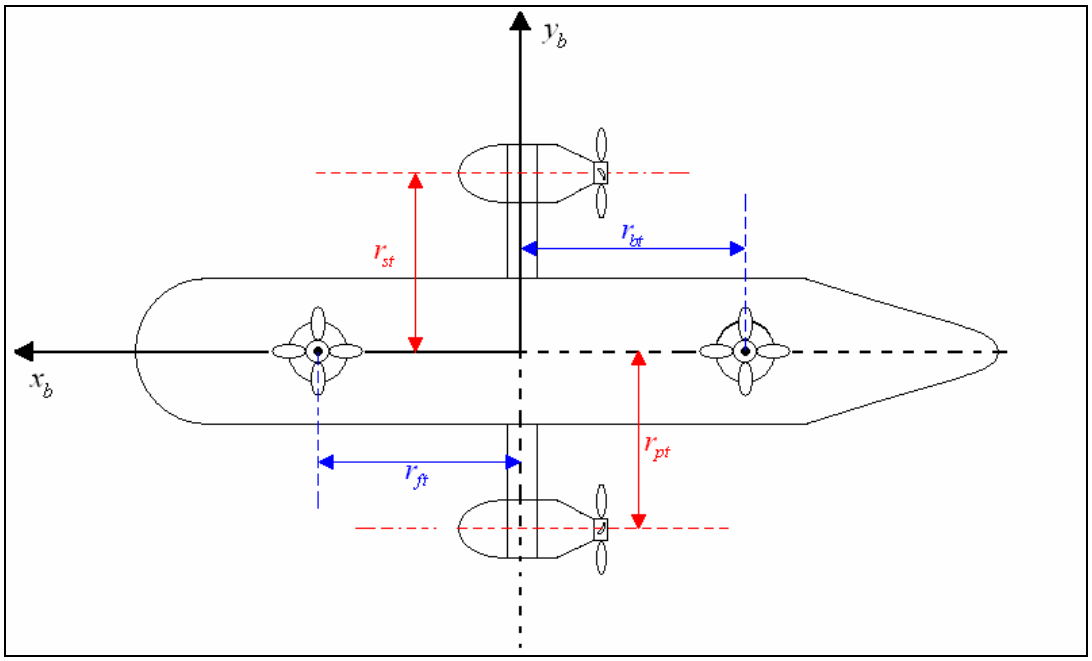

Figure 11 Top view of vehicle thrusters and their locations

2.3 Overall Equations

By combining overall force and moment calculation methods we can represent the non-linear time invariant six equation of motion as given below:

$$\begin{aligned}&\left(m-X_{\dot{u}}\right)\dot{u}+mz_g\dot{q}-my_g\dot{r}=X_{HS}+X_{u|u|}u|u|+\left(X_{wq}-m\right)wq\\&+\left(X_{qq}+mx_g\right)q^2+\left(X_{vr}+m\right)vr+\left(X_{rr}+mx_g\right)r^2-my_gpq-mz_gpr+X_T\end{aligned}$$

(2.100)

$$\begin{aligned}&\left(m-Y_{\dot{v}}\right)\dot{v}-mz_g\dot{p}+\left(mx_g-Y_{\dot{r}}\right)\dot{r}=Y_{HS}+Y_{v|v|}v|v|+Y_{r|r|}r|r|+my_gr^2\\&+\left(Y_{ur}-m\right)ur+\left(Y_{wp}+m\right)wp+\left(Y_{pq}-mx_g\right)pq+Y_{uv}uv+my_gp^2+mz_gqr\end{aligned}$$

(2.101)

$$\begin{aligned}&\left(m-Z_{\dot{w}}\right)\dot{w}+my_g\dot{p}-\left(mx_g+Z_{\dot{q}}\right)\dot{q}=Z_{HS}+Z_{w|w|}w|w|+Z_{q|q|}q|q|\\&+\left(Z_{uq}+m\right)uq+\left(Z_{vp}-m\right)vp+\left(Z_{rp}-mx_g\right)rp+Z_{uw}uw+mz_g\left(p^2+q^2\right)\\&-my_grq+Z_T\end{aligned}$$

(2.102)

$$\begin{aligned}&-mz_g\dot{v}+my_g\dot{w}+\left(I_{xx}-K_{\dot{p}}\right)\dot{p}=K_{HS}+K_{p|p|}p|p|-\left(I_{zz}-I_{yy}\right)qr\\&+m\left(uq-vp\right)-mz_g\left(wp-ur\right)K_T\end{aligned}$$

(2.103)

$$\begin{aligned}&-mz_g\dot{u}+\left(mx_g+M_{\dot{w}}\right)\dot{w}+\left(I_{yy}-M_{\dot{q}}\right)\dot{q}=M_{HS}+M_{w|w|}w|w|\\&+M_{q|q|}q|q|+\left(M_{uq}-mx_g\right)uq+\left(M_{vp}+mx_g\right)vp\\&+\left(M_{rp}-I_{xx}+I_{zz}\right)rp+mz_g\left(vr-wq\right)+M_{uw}uw+M_T\end{aligned}$$

(2.104)

$$\begin{aligned}&-my_g\dot{u}+\left(mx_g+N_{\dot{v}}\right)\dot{v}+\left(I_{zz}-N_{\dot{r}}\right)\dot{r}=N_{HS}+N_{v|v|}v|v|\\&+N_{r|r|}r|r|+\left(N_{ur}-mx_g\right)ur+\left(N_{wp}+mx_g\right)wp\\&+\left(N_{pq}-I_{yy}+I_{zz}\right)pq-my_g\left(vr-wq\right)+N_{uv}uv+N_T\end{aligned}$$

(2.105)

CHAPTER 3

CONTROLLER DESIGN

In this chapter linearization of the equation of the motion of the vehicle and the design of the control strategies are explained. Since response time of the thrusters is faster than response time of the vehicle, we considered inputs to the system are the forces and moments applied by the thrusters. So in this chapter we will first give the control strategies applied to the thrusters. After that the system equations will be decoupled and linearized. Finally, we will describe how the controllers are designed for the basic motions and how a supervisory autopilot is designed to manage the combinations of the basic motion controllers

3.1 Design of Thruster Control

A fast and robust performance for the thruster controller is a vital requirement since any protracted, unstable and erroneous behavior of thrusters will trigger alike behavior in the vehicle response. Due to the high non linearity and coupled dynamics of the thruster model, the chosen design method for the controller is using Simulink signal constraint block in Signal Response Optimization toolbox to minimize linearization errors and accomplish desired response.

Simulink Response Optimization tunes the specified parameters in the controller block to meet specified constraints in the output signal. This block provides a graphical user interface to assist controller design in the time domain. With this block, controller parameters can be tuned within a nonlinear Simulink model to meet the time domain performance requirements. These performance requirements

are defined either by graphically placing constraints within a time domain window or by defining a reference signal to be tracked.

To use the Simulink Response Optimization, the Signal Constraint block is connected to the thrust output in order to place constraints to its output signal in the Simulink model. The usage of the Signal Constraint block with thruster model is shown in Figure 12. Simulink Response Optimization converts the time domain constraints into a constrained optimization problem and solves the problem using the optimization routines taken from the Optimization Toolbox. Parameters are iteratively changed and the simulation results are compared with each other to better meet the constraint objectives.

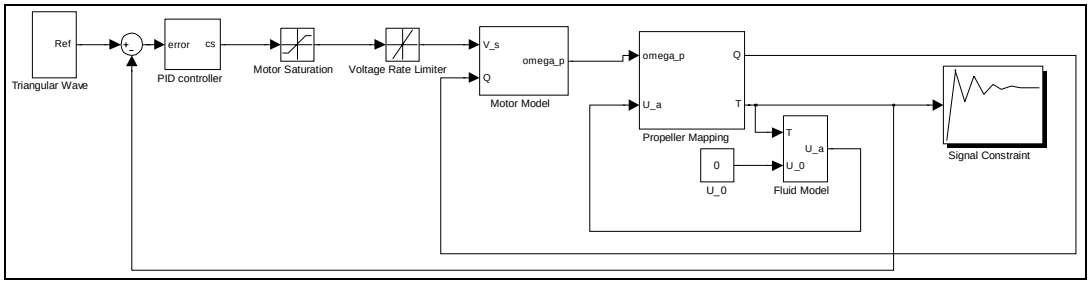

Figure 12 Thruster model and Signal Constraint Block configuration

The gain parameters of the PI controller of the thruster are defined as the tunable parameters and initialized in the MATLAB workspace. The initial values for the gain parameters are all taken as zero. Further to protect the motor from excessive control outputs we placed voltage saturator and rate limiter to the output of controller.

To adjust the constraints on the signal, the goal chosen as tracking reference signal. For the reference signal a triangular wave generated which is given in Figure 13. Final parameters of thruster parameters are given in Appendix C.

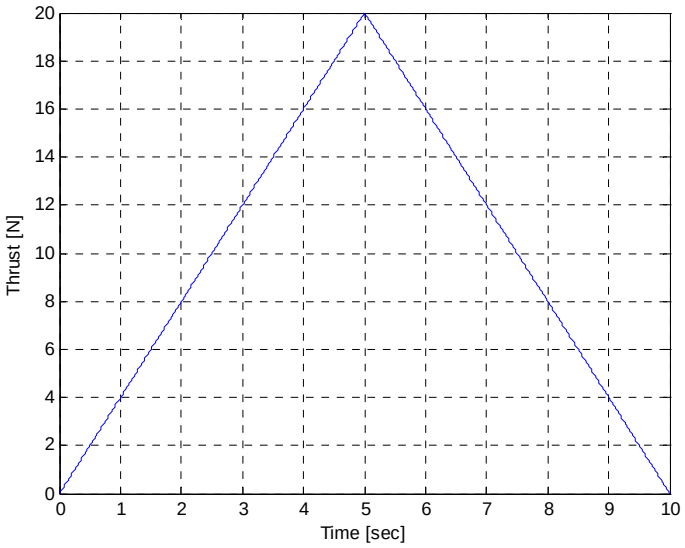

Figure 13 Reference Signal

Response of the controlled system with tuned controller parameters for this signal is given in Chapter 4.

3.2 Linearized System Models

As discussed by Healey [10], under some assumptions it is appropriate to decouple the vertical and horizontal plane motions. We will design controllers belonging to each motion type by decoupling the equations for the surge, heave/pitch and yaw motions. Effectiveness of these controllers will be tested by means of simulations, which employ complete nonlinear and coupled dynamics and include maneuvers that combine the basic motions

3.2.1 Vertical Plane Motions

The first plane which is decoupled from the remaining dynamics is vertical plane. Out of plane dynamics which are sway, roll and yaw are neglected. The assumptions made here in neglecting these terms are:

- Due to hydrostatic moment roll angle is kept very close to zero.
- The heading controller sets the yaw rates almost equal to zero.
- Sway velocity is zero

So the remaining dynamics that are going to be considered are, body-relative velocities surge and heave velocities, pitch rate, earth-relative vehicle forward position, depth, and pitch angle. Assuming that the vehicle moves only in the vertical plane and neglecting horizontal dynamics results in the following state vector;

$$\overline{x} = \begin{bmatrix} u & w & q & x & z & \theta \end{bmatrix}^T \tag{2.106}$$

In order to find state space representation of the system, general form of the equations of motion is manipulated by making some row and column removal operations. The reduced form is given below:

$$\begin{bmatrix} m - X_{\dot{u}} & 0 & mz_g \\ 0 & m - Z_{\dot{w}} & -mx_g - Z_{\dot{q}} \\ mz_g & -mx_g - M_{\dot{w}} & I_{yy} - M_{\dot{q}} \end{bmatrix} \begin{bmatrix} \dot{u} \\ \dot{w} \\ \dot{q} \end{bmatrix} = \begin{bmatrix} \sum X \\ \sum Z \\ \sum M \end{bmatrix} \tag{2.107}$$

State equations for the $\Im_e$ frame velocity components can be found by using $\Im_b$ frame velocity components and $\Im_e$ frame velocity components relations given in (2.7). These formulas are simplified due to the vertical plane assumption. Transformation matrix under absence of yaw and roll rotation is:

$$\hat{C}^{(e,b)} = \begin{bmatrix} \cos\theta & 0 & \sin\theta \\ 0 & 1 & 0 \\ -\sin\theta & 0 & \cos\theta \end{bmatrix} \tag{2.108}$$

To find $\Im_e$ frame velocity components:

$$\begin{bmatrix} \dot{x} & 0 & \dot{z} \end{bmatrix}^T = \hat{C}^{(e,b)} \begin{bmatrix} u & 0 & w \end{bmatrix}^T \tag{2.109}$$

By making multiplication $\Im_e$ velocity components are found as:

$$\dot{x} = u\cos\theta + w\sin\theta \tag{2.110}$$

$$\dot{z} = w\cos\theta - u\sin\theta \tag{2.111}$$

To find the pitch angle rate state equation we can use Euler angle rates - body angular rates relations as given in (2.13). This equation is also simplified for vertical plane motion assumption as;

$$\dot{\theta} = q \tag{2.112}$$

One last thing to do is writing the external forces applied to the vehicle using the vertical plane assumption. Starting from equations(2.100), (2.102) and(2.104), they are written as follows:

$$\sum X = X_{HS} + X_{u|u|}u|u| + \left(X_{wq} - m\right)wq + \left(X_{qq} + mx_g\right)q^2 + X_T \tag{2.113}$$

$$\begin{aligned} &\sum Z = Z_{HS} + Z_{w|w|}w|w| + Z_{q|q|}q|q| + \left(Z_{uq} + m\right)uq \cdots \\ &+Z_{uw}uw + mz_g q^2 + Z_T \end{aligned} \tag{2.114}$$

$$\begin{aligned} &\sum M = M_{HS} + M_{w|w|}w|w| + M_{q|q|}q|q| + \left(M_{uq} - mx_g\right)uq \cdots \\ &-mz_g wq + M_{uw}uw + M_T \end{aligned} \tag{2.115}$$

It can be seen that vertical plane motion consists of 2 + 1 dynamics which are two translations (surge and heave) and one rotation (pitch). It is chosen to inspect and linearize these dynamics in two groups. First the surge motion dynamics will be linearized. Subsequently the pitch and heave dynamics will be investigated. As pitch and heave dynamics take input from the same group of thrusters it is convenient to keep the pitch rotation at zero, which happens to be the natural stabilization position due to the longitudinal hydrostatic moment.

3.2.1.1 Surge Motion

To obtain state space model equations (2.110) and (2.113) have to be linearized. The strategy chosen is to decouple depth and surge motion is to make the depth controller to command zero pitch angle. Additional assumptions made to linearize surge dynamics are represented below:

- Surge velocity (u) does not deviate significantly around a chosen velocity U_0
- Depth controller is capable of setting the pitch angle and the heave velocity perfectly to zero.

Linearization is carried out with given assumptions to obtain linear system state space model. The decoupled states of surge motion are given below:

$$\bar{x} = \begin{bmatrix} u & x \end{bmatrix}^T \tag{2.116}$$

First linearization is carried out for obtaining state equation for surge velocity. The linearization reference for the perturbed surge velocity is U_0 i.e.

$$u = u' + U_0 \tag{2.117}$$

And the perturbed state derivative is given as:

$$\dot{u} = \dot{u}' \tag{2.118}$$

From the vertical plane dynamics, the reduced equation of motion for the surge motion can be found from (2.107) and (2.113) as:

$$\left(m - X_{\dot{u}}\right)\dot{u} = \sum X \tag{2.119}$$

$$\sum X = X_{HS} + X_{u|u|} u\left|u\right| + X_T \tag{2.120}$$

In equations (2.120) given hydrostatic force can be represented as;

$$X_{HS} = \left(B - W\right)\sin\theta \approx 0 \tag{2.121}$$

Assuming forward motion the cross flow drag force calculation in equation (2.120) can be written as $X_{u|u|}u^2$. Applying change of variables:

$$u^2 = \underbrace{u'^2}_{\approx 0} + 2U_0 u' + {U_0}^2 \approx 2U_0 u' + {U_0}^2 \tag{2.122}$$

The constant term ${U_0}^2$ can be specified as steady state forcing and omit from here to take place in the bias term for added to thrusts commanded in velocity controller.

Input forces can be decomposed into axial forces of two thrusters which is given in (2.99).

$$X_T = T_{st} + T_{pt} \tag{2.123}$$

Since port and starboard thrusters are identical and will be worked synchronously, they can be lumped into one input and denoted as T_{surge}. The linearized equation of motion can be written as;

$$\left(m - X_{\dot{u}}\right)\dot{u}' = X_{u|u|} 2U_0 u' + T_{surge} \tag{2.124}$$

Dividing both sides with inverse of added mass term will result in state equation.

$$\dot{u}' = \frac{X_{u|u|}2U_0}{m - X_{\dot{u}}}u' + \frac{1}{m - X_{\dot{u}}}T_{surge} \tag{2.125}$$

The given state equation can be used to implement the surge velocity controller. To carry out with surge velocity controller design, reference velocity U_0 has to be set to desired value. Alternatively position controller can be designed by setting U_0 to zero. And reference position X_0 is taken as the desired location. Perturbed position earth fixed reference frame is expressed as

$$x = x' + X_0 \tag{2.126}$$

And perturbed state derivative is:

$$\dot{x} = u' \tag{2.127}$$

Taking (2.125) and (2.127), then letting stability velocity U_0 as zero will result in the following linearized time invariant state space model.

$$\begin{bmatrix} \dot{u}' \\ \dot{x}' \end{bmatrix} = \begin{bmatrix} 0 & 0 \\ 1 & 0 \end{bmatrix} \begin{bmatrix} u' \\ x' \end{bmatrix} + \begin{bmatrix} \frac{1}{m - X_{\dot{u}}} \\ 0 \end{bmatrix} T_{surge} \tag{2.128}$$

3.2.1.2 Heave and Pitch Motion

After the surge motion state space model is attained as described above; heave and pitch motion linearization can be performed with a similar methodology. For this purpose the following assumptions are made:

- Heave velocity (*w*) does not deviate significantly around chosen velocity W_0
- Surge controller is capable of setting surge velocity to zero.

For heave/pitch motion control our state matrix is;

$$\bar{x} = \begin{bmatrix} w & q & z & \theta \end{bmatrix}^T \tag{2.129}$$

In an analogous way, first heave velocity and pitch rate state equations will be given. Our perturbed states are chosen as:

$$w = w' + W_0 \tag{2.130}$$

$$q = q' \tag{2.131}$$

$$\theta = \theta' \tag{2.132}$$

As it is stated above the desired motion for the vehicle is to change depth while keeping the pitch angle zero. Therefore, pitch rate and pitch angle perturbations are given around zero.

Applying these assumptions will lead to given state equation:

$$\dot{w} = \dot{w}' \tag{2.133}$$

$$\dot{q} = \dot{q}' \tag{2.134}$$

$$\dot{\theta} = q' \tag{2.135}$$

Combining (2.114) and (2.115):

$$\begin{bmatrix} m - Z_{\dot{w}} & -mx_g - Z_{\dot{q}} \\ -mx_g - M_{\dot{w}} & I_{yy} - M_{\dot{q}} \end{bmatrix} \begin{bmatrix} \dot{w} \\ \dot{q} \end{bmatrix} = \begin{bmatrix} \sum Z \\ \sum M \end{bmatrix} \tag{2.136}$$

$$\sum Z = Z_{HS} + Z_{w|w|} w|w| + Z_T \tag{2.137}$$

$$\sum M = M_{HS} + M_T \tag{2.138}$$

In equations (2.137) and (2.138) given hydrostatic force and moment can be represented as;

$$Z_{HS} = \left(W - B\right) \tag{2.139}$$

And multiply force with the moment arm.

$$M_{HS} = -z_g W \sin\theta \tag{2.140}$$

Assuming heave cross flow drag force calculation in equation (2.137) can be written as $Z_{w|w|}w^2$, and changing variables with perturbed velocity:

$$w^2 = \underbrace{w'^2}_{\approx 0} + 2W_0 w' + W_0{}^2 = 2W_0 w' + W_0{}^2 \tag{2.141}$$

and for $\sin\theta$ using Taylor expansion around $\theta = 0$ and taking first two terms result in linearized force equations as;

$$\sum Z = mg - B + Z_{w|w|}\left(2W_0 w' + W_0{}^2\right) + Z_T \tag{2.142}$$

$$\sum M = -z_g mg\theta' + M_T \tag{2.143}$$

The constant terms $W_0{}^2$ and $\left(W - B\right)$ can be specified as steady state forcing and omit from here to take place in the bias term of controller.

Using thruster input force relations given in (2.99)

$$Z_T = T_{ft} + T_{bt} \tag{2.144}$$

$$M_T = T_{bt} r_{bt,1} - T_{ft} r_{ft,1} \tag{2.145}$$

Linearized dynamic equations can be written as

$$\begin{bmatrix} m-Z_{\dot{w}} & -mx_g-Z_{\dot{q}} \\ -mx_g-M_{\dot{w}} & I_{yy}-M_{\dot{q}} \end{bmatrix}\begin{bmatrix} \dot{w}' \\ \dot{q}' \end{bmatrix}=\begin{bmatrix} Z_{w|w|}2W_0w' \\ -z_g mg\theta' \end{bmatrix}+\cdots \\ \begin{bmatrix} 1 & 1 \\ -r_{ft,1} & r_{bt,1} \end{bmatrix}\begin{bmatrix} T_{ft} \\ T_{bt} \end{bmatrix} \tag{2.146}$$

Multiplication of both sides with the inverse of the reduced mass matrix will give two state equations:

$$\begin{bmatrix} \dot{w}' \\ \dot{q}' \end{bmatrix}=\begin{bmatrix} m-Z_{\dot{w}} & -mx_g-Z_{\dot{q}} \\ -mx_g-M_{\dot{w}} & I_{yy}-M_{\dot{q}} \end{bmatrix}^{-1}\left\{\begin{bmatrix} Z_{w|w|}2W_0w' \\ -z_g mg\theta' \end{bmatrix}+\cdots \right. \\ \left.\begin{bmatrix} 1 & 1 \\ -r_{ft,1} & r_{bt,1} \end{bmatrix}\begin{bmatrix} T_{ft} \\ T_{bt} \end{bmatrix}\right\} \tag{2.147}$$

After the necessary manipulations, the state equations for the heave velocity and the pitch rate are obtained as

:

$$\begin{bmatrix} \dot{w}' \\ \dot{q}' \\ \dot{\theta}' \end{bmatrix}=\underline{A}_{3\times 3}\begin{bmatrix} w' \\ q' \\ \theta \end{bmatrix}+\underline{B}_{2\times 3}\begin{bmatrix} T_{ft} \\ T_{bt} \end{bmatrix} \tag{2.148}$$

One can use the given state equation to design the heave velocity and pitch rate controller respectively. For the heave velocity controller the reference velocity W_0 set to a desired value. To obtain the position controller W_0 is set to zero and a reference depth Z_0 is introduced. Perturbed depth and depth rate are given below.

$$\dot{z}=w' \tag{2.149}$$

$$z=z'+Z_0 \tag{2.150}$$

To find state equations for depth, matrix multiplication given in (2.147) is done again with zero heave velocity.

$$\begin{bmatrix} \dot{w}' \\ \dot{q}' \end{bmatrix} = \begin{bmatrix} m - Z_{\dot{w}} & -mx_g - Z_{\dot{q}} \\ -mx_g - M_{\dot{w}} & I_{yy} - M_{\dot{q}} \end{bmatrix}^{-1} \left\{ \begin{bmatrix} 0 \\ -z_g mg\theta' \end{bmatrix} + \cdots \right.$$
$$\left. \begin{bmatrix} 1 & 1 \\ -r_{ft,1} & r_{bt,1} \end{bmatrix} \begin{bmatrix} T_{ft} \\ T_{bt} \end{bmatrix} \right\} \tag{2.151}$$

Finally the state equations for the depth controller are obtained as:

$$\begin{bmatrix} \dot{w}' \\ \dot{q}' \\ \dot{\theta}' \\ \dot{z}' \end{bmatrix} = \underline{A}_{4\times4} \begin{bmatrix} w' \\ q' \\ \theta \\ z' \end{bmatrix} + \underline{B}_{2\times4} \begin{bmatrix} T_{ft} \\ T_{bt} \end{bmatrix} \tag{2.152}$$

3.2.2 Horizontal Plane

In horizontal plane a similar approach is used which is represented in the vertical plane linearization procedure. Main assumptions in horizontal plane decoupling are:

- Out of plane dynamics which involve pitch, surge and heave motions are set to zero
    - Pitch angle, pitch rate and heave velocity are set to zero by a perfect depth controller.
    - Surge velocity is set to zero by a perfect surge controller.
- Due to hydrostatic moment, roll angle has settled to zero
- Sway velocity is zero

This time the reduced state vector is only composed of yaw rate and yaw angle:

$$\bar{x} = \begin{bmatrix} r & \psi \end{bmatrix}^T \tag{2.153}$$

In order to find the state space representation for the yaw dynamics the sixth row of the general form of the equation of motion is taken and reduced to the following form:

$$\left[I_{zz} - N_{\dot{r}}\right]\left[\dot{r}\right] = \sum N \tag{2.154}$$

To find the state equations for the yaw angle rate equation (2.12) is used. Because pf the plane motion assumption ($\phi = 0$ and $\theta = 0$), that equation reduces to:

$$\dot{\psi} = r \tag{2.155}$$

The next thing to do is writing the external moment applied to the vehicle using the horizontal plane assumption. Taking equation (2.105) and omitting the out off plane terms:

$$\sum N = N_{HS} + N_{r|r|} r\left|r\right| + N_T \tag{2.156}$$

Due to the horizontal plane assumption the hydrostatic moment term N_{HS} does not exist. As done above to linearize the system and find the state equitation, perturbed velocities are used. Yaw rate is assumed to be perturbed around a constant nominal yaw rate R_0, and yaw angle is perturbed around a target value Ψ_0.

$$r = R_0 + r' \tag{2.157}$$

$$\dot{r} = \dot{r}' \tag{2.158}$$

$$\sum N = N_{r|r|}\left(2R_0 r' + {R_0}^2\right) + N_T \tag{2.159}$$

The term $N_{r|r|}{R_0}^2$ is a bias term which can be added onto the controller input when the vehicle commanded to make a rotation around z_b with a constant angular rate R_0.

The input moment can be represented by the net moment produced by the port and the starboard thrusters. We will take the sixth column of the input thrust net moment relations stated in (2.99):

$$N_T = T_{pt} r_{pt,2} - T_{st} r_{st,2} \tag{2.160}$$

Replacing the yaw moment due to the thruster inputs to the system and changing the states with the perturbed ones, will result in:

$$\left[I_{zz} - N_{\dot{r}}\right]\left[\dot{r}'\right] = \left[2N_{r|r|}R_0\right]\left[r'\right] + \begin{bmatrix} -r_{st,2} & r_{pt,2} \end{bmatrix}\begin{bmatrix} T_{st} \\ T_{pt} \end{bmatrix} \tag{2.161}$$

Dividing both sides with added inertia term will lead to the yaw rate state equation as:

$$\left[\dot{r}'\right] = \begin{bmatrix} \dfrac{2N_{r|r|}R_0}{I_{zz} - N_{\dot{r}}} \end{bmatrix}\left[r'\right] + \begin{bmatrix} \dfrac{-r_{st,2}}{I_{zz} - N_{\dot{r}}} & \dfrac{r_{pt,2}}{I_{zz} - N_{\dot{r}}} \end{bmatrix}\begin{bmatrix} T_{st} \\ T_{pt} \end{bmatrix} \tag{2.162}$$

To find the yaw angle state space model, the yaw rate is set to zero. The perturbed yaw angle state and its derivative are given as:

$$\psi = \psi' + \Psi_0 \tag{2.163}$$

$$\dot{\psi} = r' \tag{2.164}$$

Setting the yaw rate to zero in (2.162) and combining with (2.164) the yaw angle state space model can be obtained as:

$$\begin{bmatrix} \dot{r} \\ \dot{\psi} \end{bmatrix} = \begin{bmatrix} 0 & 0 \\ 1 & 0 \end{bmatrix}\begin{bmatrix} r \\ \psi \end{bmatrix} + \begin{bmatrix} \dfrac{-r_{st,2}}{I_{zz} - N_{\dot{r}}} & \dfrac{r_{pt,2}}{I_{zz} - N_{\dot{r}}} \\ 0 & 0 \end{bmatrix}\begin{bmatrix} T_{st} \\ T_{pt} \end{bmatrix} \tag{2.165}$$

3.2.3 Choosing Control Strategy

The chosen strategy for controlling the motions described above is the state feedback approach, which gives the control input as

$$\overline{u} = K\overline{x} \tag{2.166}$$

To find the feedback gain matrix the linear quadratic regulator approach is used to satisfy the optimality of the feedback control.

Performance index for LQR problem can be defined as;

$$J = \int_0^{t_f} \left(\overline{x}^T Q \overline{x} + \overline{u}^T R \overline{u} \right) d\tau \tag{2.167}$$

where the state weighting matrix Q is real, symmetric and positive definite or positive semi-definite while the and control weighting matrix R is real, symmetric and positive definite.

If a unique positive definite solution for P exists to the following algebraic Riccati equation,

$$Q - A^T R + RA - RBP^{-1}B^T R = 0\,, \tag{2.168}$$

then the linear state feedback control law in (2.166) results in the minimization of J. The minimization of J implies a desire to minimize both excessive output excursions and the control effort required to prevent such excursions. The adjustable weights $\boldsymbol{Q}$, and $\boldsymbol{R}$ can be used to obtain an appropriate compromise between these two conflicting goals. The optimal control gain for this problem then becomes

$$K = P^{-1}B^t R \tag{2.169}$$

The weighting matrices are given below for the controllers of the surge, heave/pitch and yaw motions.

The surge position controller weighting matrices are chosen in order to minimize position error. The control effort weighting is decreased in order to minimize settling time for position. To reduce over-shoot in position, the weighting for the surge velocity is kept in the same order with the position weighting to prevent high velocities during the transition phase.

$$Q_{surge} = \begin{bmatrix} 1 & 0 \\ 0 & 1 \end{bmatrix} \tag{2.170}$$

$$R_{surge} = \begin{bmatrix} 0.1 \end{bmatrix} \tag{2.171}$$

The heave controller weighting matrices are chosen in order to minimize the depth error. As stated in the surge position control, input penalties are reduced to achieve faster response. The heave velocity weighting is essential to avoid over-shoot in the depth position. The pitch rate and pitch angle weightings are taken smaller than those of the heave velocity and depth since the longitudinal hydrostatic moment and the high pitch damping ensure the stabilization of these states. By taking these weightings smaller the excessive pitch control effort is prevented.

$$Q_{yaw} = \begin{bmatrix} 1 & 0 & 0 & 0 \\ 0 & 0.1 & 0 & 0 \\ 0 & 0 & 0.1 & 0 \\ 0 & 0 & 0 & 1 \end{bmatrix} \tag{2.172}$$

$$R_{heave} = \begin{bmatrix} 0.1 & 0 \\ 0 & 0.1 \end{bmatrix} \tag{2.173}$$

The yaw controller weighting matrices are also similarly chosen to reduce the yaw angle error. Once more the input penalties are decreased to achieve faster response. The yaw rate weighting is kept higher to place a damping effect on the yaw control.

$$Q_{surge} = \begin{bmatrix} 1 & 0 \\ 0 & 1 \end{bmatrix} \tag{2.174}$$

$$R_{yaw} = \begin{bmatrix} 0.1 & 0 \\ 0 & 0.1 \end{bmatrix} \tag{2.175}$$

3.3 Autopilot

As we stated above the designed controllers with thrusters are only capable of controlling the vehicle in four degrees of freedom. So in order to provide a coordination of the yaw and surge controllers to achieve a combined maneuver of the vehicle in horizontal plane we add a line-of-sight autopilot that works on the yaw angle and position error signal.

Furthermore we improved the performance of the system by posing of some limitations to prevent excessive controller inputs and to stop the surge and/or the yaw controllers whenever necessary in order to avoid entering the coupled regions of planar dynamics where our controller design assumptions do not hold. These limitations are given below and one can examine the flow of these checks and related actions taken in Figure 14:

1. If the vehicle roll angle (ϕ) exceeds allowable roll angle the port and starboard thrusters are set to wait for t_{wait} seconds for the stabilization of the roll angle

2. To prevent excessive yaw command near the target location, yaw error set to zero when vehicle reaches a close neighborhood of the target point.

3. Than if magnitude of the difference in positions of the vehicle and the target is greater than the predefined distance, yaw error check occurs. If the yaw angle is greater than a predefined maximum error, the vehicle position error

is set to zero to avoid the motion in surge in an incorrect direction. Afterwards the vehicle starts a turning maneuver.

4. Finally the yaw error is checked. If it is greater than π the vehicle is set to turn in the reverse direction.

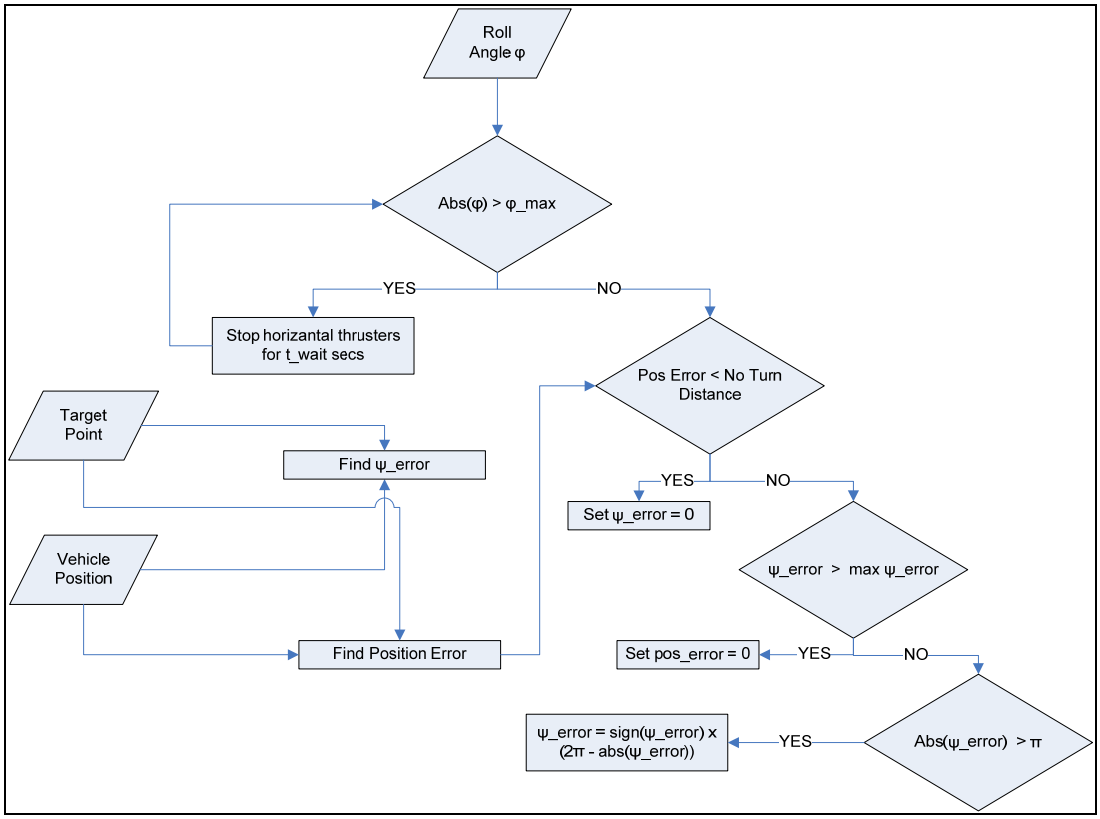

Figure 14 Flow diagram of the autopilot

CHAPTER 4

SAMPLE TEST CASE AND RESULTS

In this chapter the simulation results will be given for some sample test cases. Simulations are conducted with the given data in this chapter.

4.1 Vehicle Used in Simulations

To test the dynamics models and control methodology, a sample vehicle data is needed. In this section the vehicle configuration and data set calculated will be introduced.

The example unmanned underwater chosen is based on the ULISAR vehicle which is in its preliminary design stage. Therefore some needed parameters for our calculations are missing. To overcome this problem missing parameters are taken from the shape similitude of this vehicle to REMUS (Figure 1). Radial geometrical parameters are normalized with diameter ratio and longitudinal parameters are normalized with length ratio.

4.1.1 Vehicle Shape

The hull shape of the vehicle is based on the Myring hull profile equations. This shape is based on fineness ratio of the body and gives the radial contour of the hull from principal axis of symmetry. Shape of the nose section is given as:

$$r(x) = \frac{1}{2} d \left[1 - \frac{x + a_{offset} - a}{a} \right]^{n^{-1}} \tag{3.1}$$

For the tail section hull radius can be found as:

$$r(x) = \frac{1}{2}d - \left[\frac{3d}{2c^2} - \frac{\tan\theta_{tail}}{c}\right](x-l)^2 + \left[\frac{d}{c^3} - \frac{\tan\theta_{tail}}{c^2}\right](x-l_f)^3 \qquad (3.2)$$

Table 2 Myring Variables for Sample Vehicle

Parameter	Value	Units
a	0.223	m
a_{offset}	0.0199	m
b	0.78677	m
c	0.65	m
c_{offset}	0.0442	m
n	2	-
θ_{tail}	0.436	rad
d	0.3	m
l_f	0.996	m
l	1.6	m

4.1.2 Physical Properties of the Vehicle

The physical parameters like mass, volume and inertial parameters are find on the design procedure. So in this work estimated values are taken for these values.

Below is given the inertial and buoyancy variables used in our calculations.

Table 3 Mass and Weight of the Sample Vehicle

Parameter	Value	Units
Mass	64	kg
Weight	627.84	N
Buoyancy	634.12	N

The center of gravity of the vehicle is located with respect to origin of body fixed coordinate system as:

Table 4 Center of gravity position with respect to origin of $\Im_b$

Parameter	Value	Units
x_g	0	m
y_g	0	m
z_g	0.08	m

The vehicle inertia tensor is defined with respect to the body-fixed origin at the vehicle center of buoyancy. It is assumed that the vehicle has two axial planes of symmetry. Therefore the off diagonal terms of inertia dyadic (I_{xy}, I_{xz}, I_{yz}) are taken

as zero. Diagonal terms of the inertia matrix are estimated by using the inertia terms of the similitude ellipsoid which has the same length, diameter and mass with the vehicle.

Table 5 Elements of Inertia Dyadic

Parameter	Value	Units
I_{xx}	1.7861	kg m^2
I_{yy}	10.326	kg m^2
I_{zz}	10.326	kg m^2

4.1.3 Thruster Properties

The vehicle uses four of the SeaBotix thrusters. The specifications of these thrusters are given in Table 6

Table 6 Thruster parameters

Parameter	Value	Unit	Description
R_p	0.038	m	Propeller radius
p	30	deg	Pitch angle of blades
$C_{L_{\max}}$	0.9	-	Maximum value for harmonic lift coefficient

Table 6 (continued) Thruster parameters

Parameter	Value	Unit	Description
$C_{D_{\max}}$	1.2	-	Maximum value for harmonic drag coefficient
γ	0.7	-	Effective added mass ratio
$\Delta\beta$	0.2	-	Momentum coefficient

Positions of the thruster with respect to $\Im_b$ are given as

$$\begin{aligned}
\left\{\vec{r}_{st}\right\}^{(b)} &= \begin{bmatrix} 0 & 0.1 & 0 \end{bmatrix}' \\
\left\{\vec{r}_{pt}\right\}^{(b)} &= \begin{bmatrix} 0 & -0.1 & 0 \end{bmatrix}' \\
\left\{\vec{r}_{bt}\right\}^{(b)} &= \begin{bmatrix} -0.5 & 0 & 0 \end{bmatrix}' \\
\left\{\vec{r}_{ft}\right\}^{(b)} &= \begin{bmatrix} 0.5 & 0 & 0 \end{bmatrix}'
\end{aligned} \tag{3.3}$$

4.2 Thruster Response Test Case

As we stated above we set the vehicle state space models by taking the thruster forces as the inputs. We assumed that the response time of the thrusters to a commanded thrust is faster than the response time of the vehicle to the thrust force and the moment

In this case we examine the response of a thruster under different input signals. First we examined the response of the thruster to a triangular test wave which is used in design of the thruster controller.

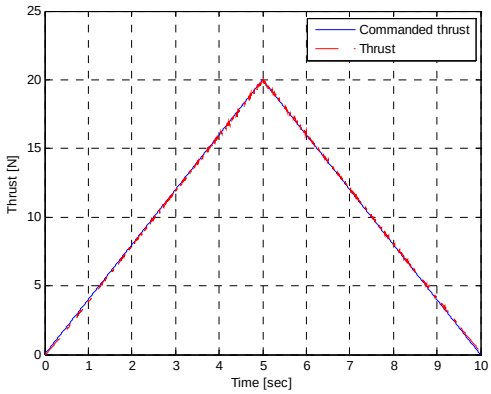

Figure 15 Thruster Triangular Wave Test Results

As we can see from Figure 15, the thruster tracks the reference signal successfully. We also used an input of sinusoidal wave that has a frequency of 0.2 Hz and amplitude of 10 N for the second test.

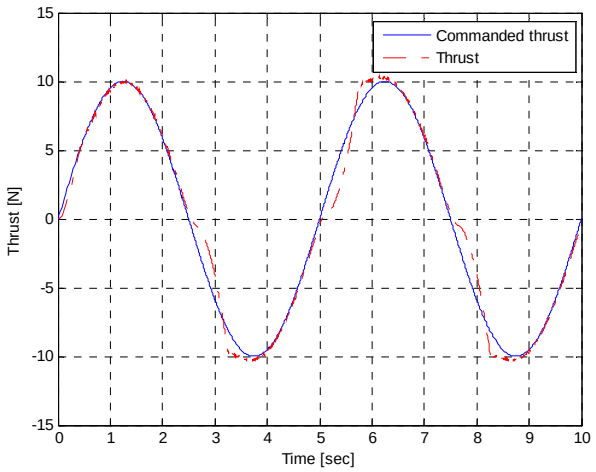

Figure 16 Thruster Sinusoidal Wave Test Results

One can observe that the output thrust of the system can follow smoothly the wave till the commanded thrust begins to change sign. Since derivative of the sinusoidal

wave gets large in that region, the output of the controller is saturated and limited. In Figure 17, in the first graph the controller output voltage and input to the thruster is given. In the second graph response of the thruster is shown after the output of controller is directly fed to the thruster.

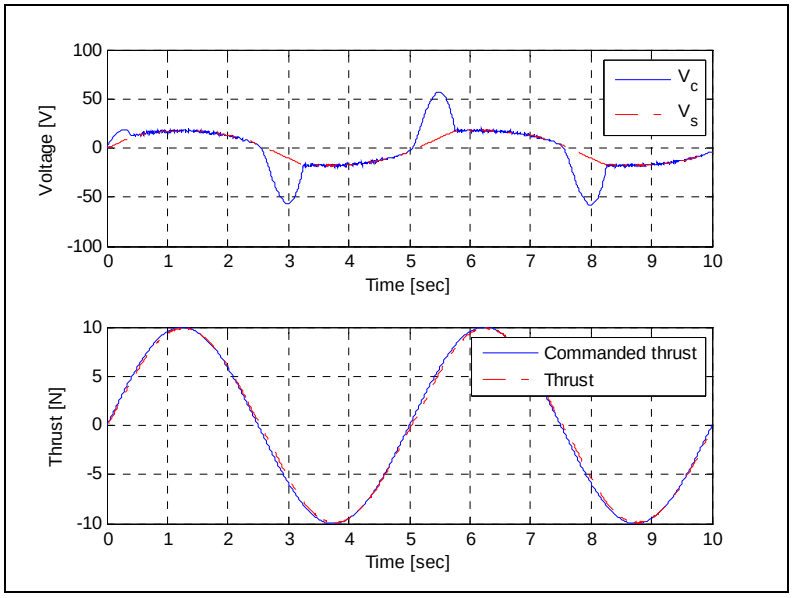

Figure 17 Voltage before and after limiters and thrust curves after deleting limiters

So the deficiencies in the response given in Figure 16 are due to the voltage saturator and the rate limiter. When these discontinuities are removed from the system output thrust successfully tracks the desired input as given in Figure 17.

4.3 Maneuver Tests

4.3.1 Forward Motion with Constant Depth

In this test the target point is located on the x axis of the earth fixed reference frame. During its course to the target point, it is wanted to keep its depth. So the desired response of the vehicle is specified as the commanded state matrix which is given below.

$$\bar{x}_c = \begin{bmatrix} u_c & w_c & q_c & x_c & z_c & \theta_c \end{bmatrix}^T = \begin{bmatrix} 0 & 0 & 0 & 30 & 0 & 0 \end{bmatrix}^T \tag{3.4}$$

The results are shown in Figure 18. The vehicle reached its goal point with a slight overshoot.

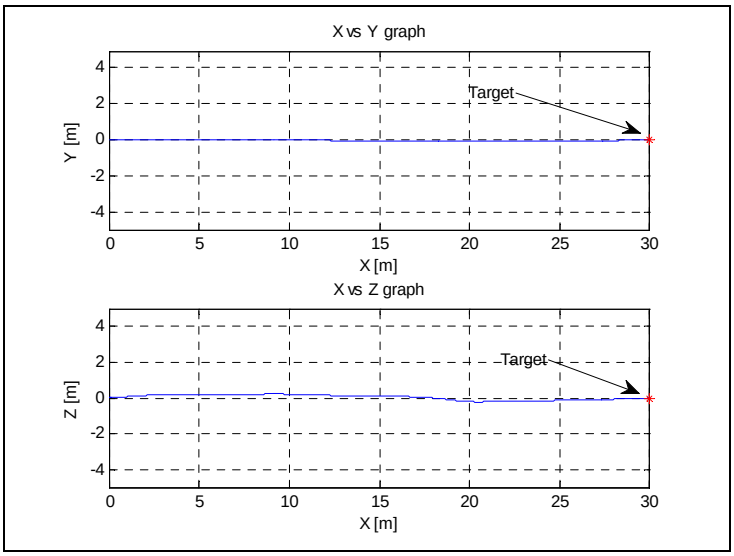

Figure 18 Position of the vehicle in earth fixed frame

Thrust time graphs are shown in Figure 19.

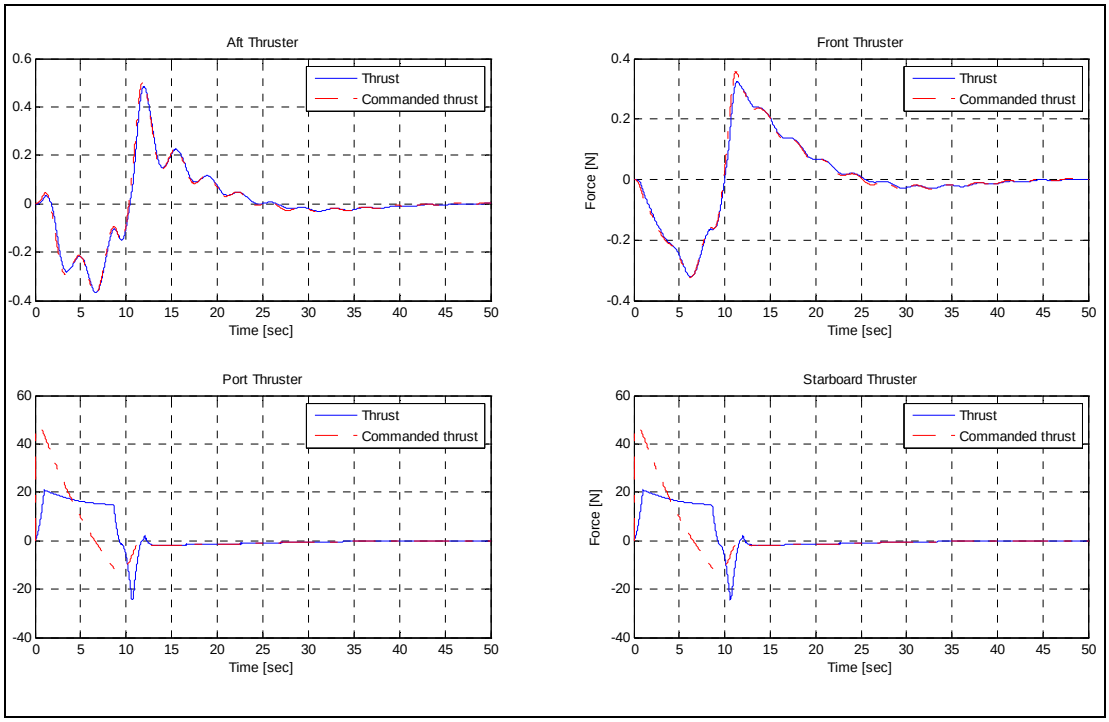

Figure 19 Thrust Time graphs

Between 0-10 seconds the port and starboard thrusters tried to minimize the position error (Figure 19) and worked together. This effect induces a roll angle. The static restoring effect of weight moment can be easily seen by looking at the roll angle ϕ shown in Figure 20.

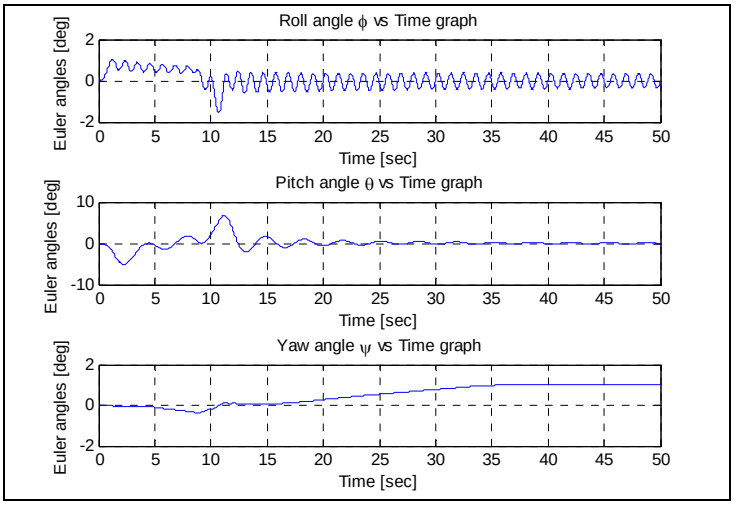

Figure 20 Euler angles versus time plot

To check our linearization assumptions, the body velocity components can be investigated. From Figure 20 and Figure 21 it can be seen that, during the surge position controller commands the port and the starboard thrusters, the heave and sway velocities, and, the Euler angles are small enough to keep the validity of the decoupling and linearization assumptions of the equations of motions.

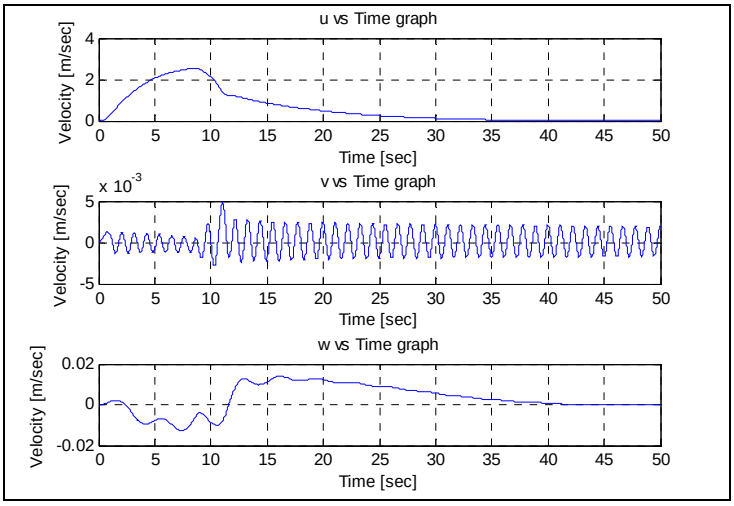

Figure 21 Body velocity components

4.3.2 Forward Motion with Change in Depth

In this test case the desired response is specified as the commanded state matrix which is given below.

$$\bar{x}_c = \begin{bmatrix} u_c & w_c & q_c & x_c & z_c & \theta_c \end{bmatrix}^T = \begin{bmatrix} 0 & 0 & 0 & 10 & 10 & 0 \end{bmatrix}^T \qquad (3.5)$$

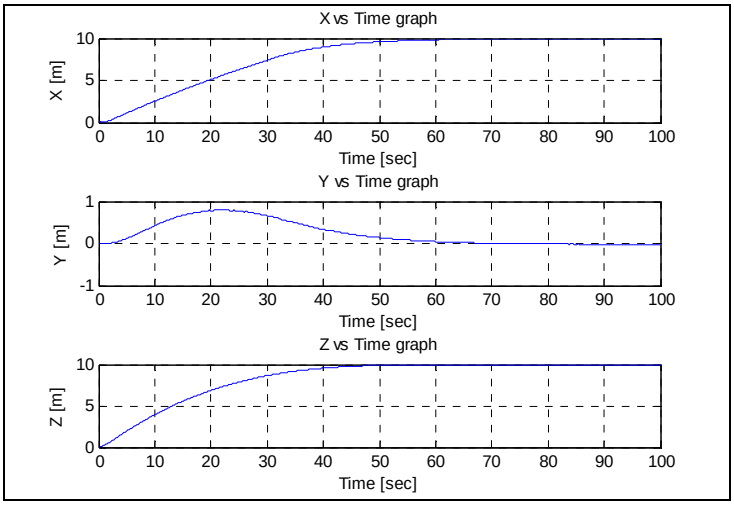

Figure 22 Earth fixed coordinates of vehicle with respect to time

Due to the depth change, front and aft controllers command more thrust (Figure 24) than the first scenario. Therefore it can be seen from Figure 22 and Figure 23 that the vehicle experiences greater yaw and position change in *y* coordinate. Also as a result of the initial high thrust input from the port and the starboard thrusters, combined with the coupled motion of the yaw-roll dynamics, the roll angle of the vehicle get oscillator under the effect of the restoring moment (Figure 23).

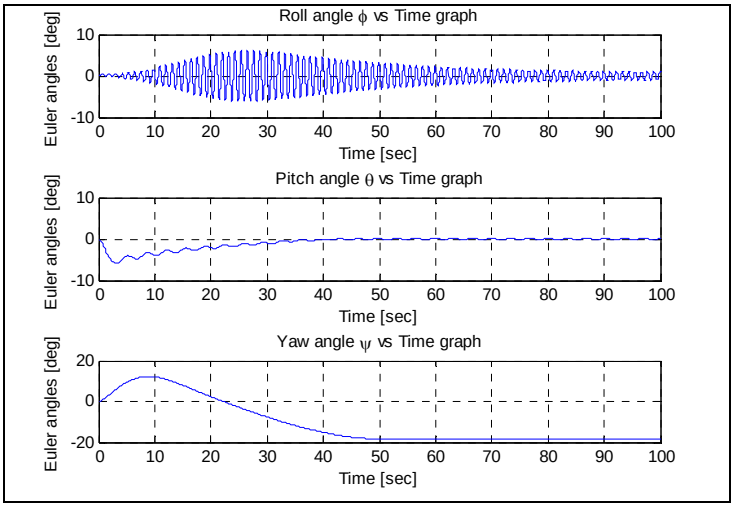

Figure 23 Euler Angles versus time plot

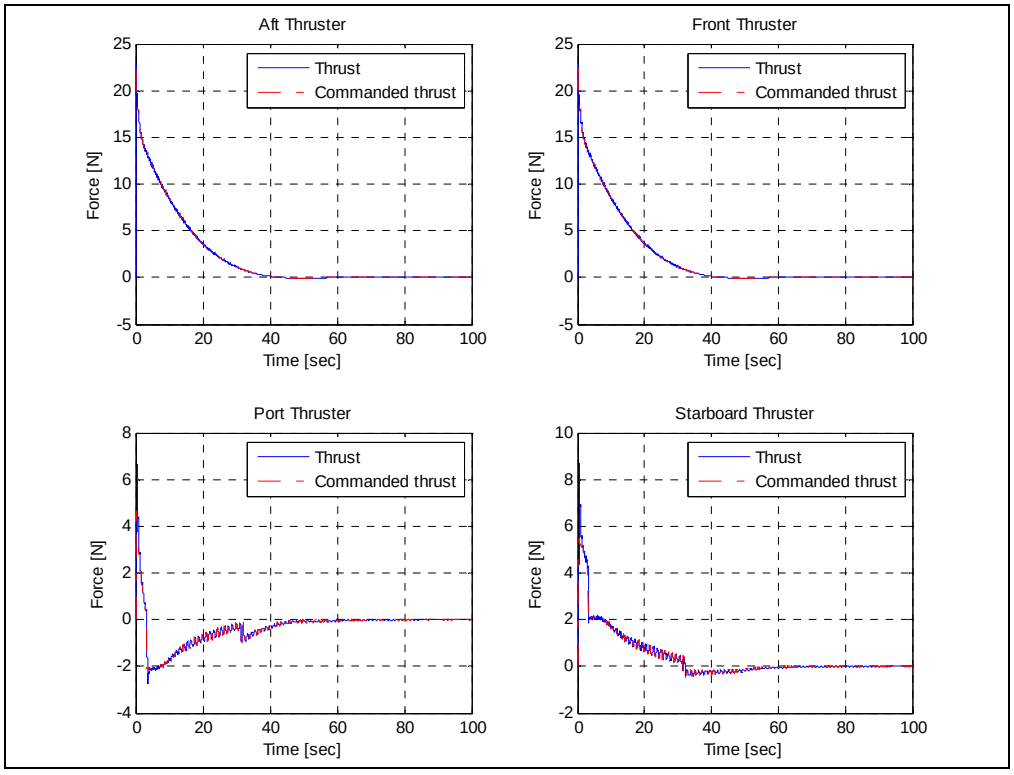

Figure 24 Thrust Time graphs

4.3.3 Position Control with Changing Depth

The aim of this test is to locate the vehicle at a desired location with a depth change. The chosen location is [0m, 10m] in the *x*-*y* plane of the earth fixed reference frame with a depth change of 10 meters. The vehicle will make a tight turn to minimize the line of sight error and than change its position to reach the desired location and depth. The desired response is specified as:

$$\bar{x}_c = \begin{bmatrix} u_c & w_c & q_c & x_c & y_c & z_c & \theta_c \end{bmatrix}^T = \begin{bmatrix} 0 & 0 & 0 & 0 & 10 & 10 & 0 \end{bmatrix}^T \quad (3.6)$$

The simulation results are given in Figure 25-Figure 27:

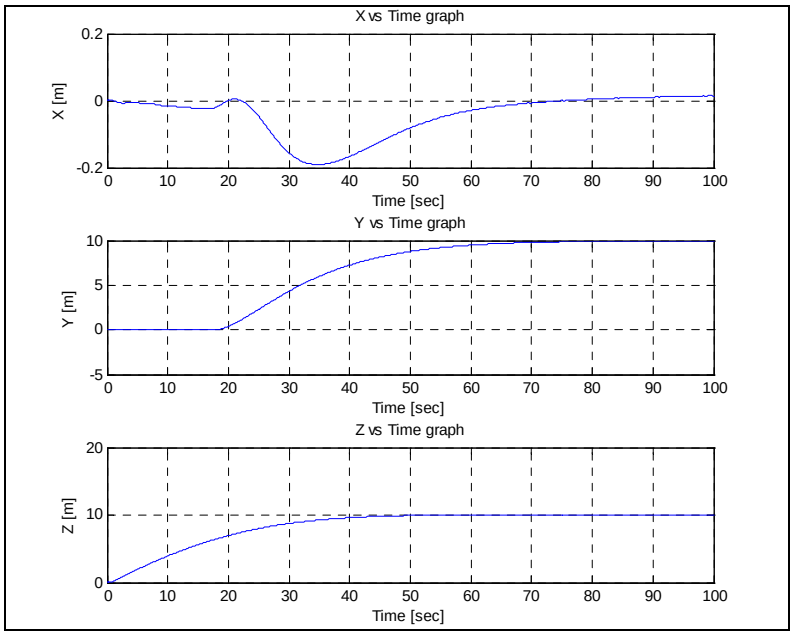

Figure 25 Earth fixed coordinates of the vehicle

As predicted the vehicle first complete the yaw turn of its motion. Then it covered the distance to the desired location.

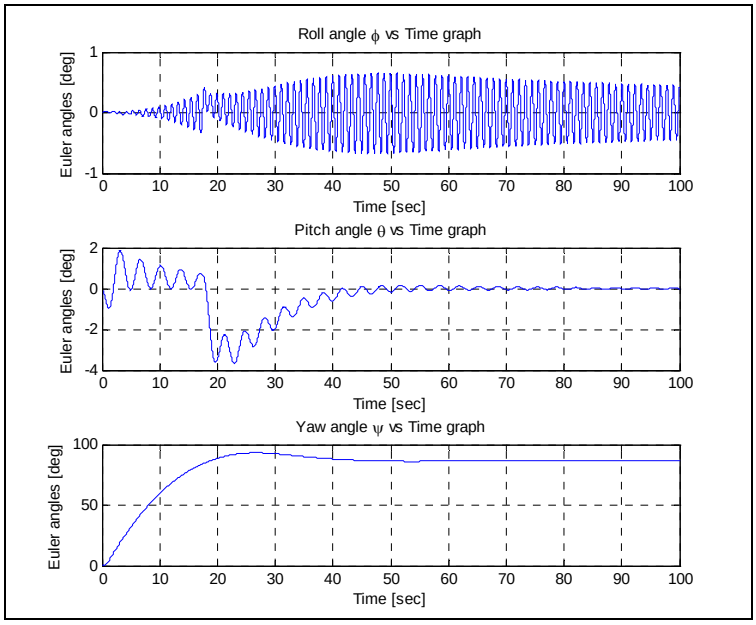

Figure 26 Euler Angles

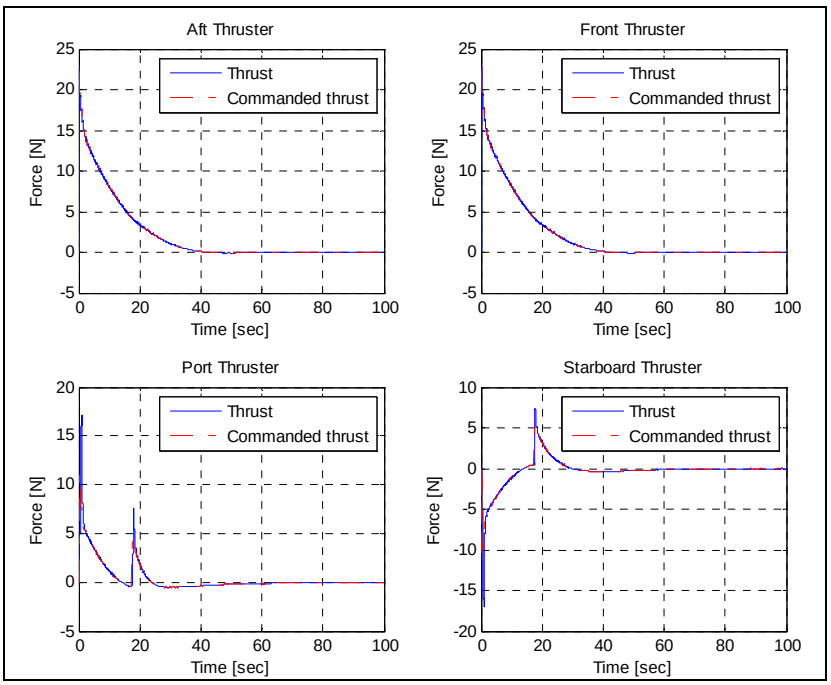

Figure 27 Thrust Forces

4.4 Effect of Underwater Currents:

In this case the vehicle is tested with an underwater current. The velocity of the current is constant and in the direction of the positive *y* axis. The velocity of the current can be specified as;

$$\{\vec{v}_{cur}\}^{(e)} = [0 \quad -0.1 \quad 0]' \tag{3.7}$$

The vehicle is required to locate itself on the *x* axis 10 meters further away the origin. This command is specified as;

$$\bar{x}_c = [u_c \quad w_c \quad q_c \quad x_c \quad z_c \quad \theta_c]^T = [0 \quad 0 \quad 0 \quad 10 \quad 0 \quad 0]^T \tag{3.8}$$

The simulation results are shown in Figure 28 and Figure 29

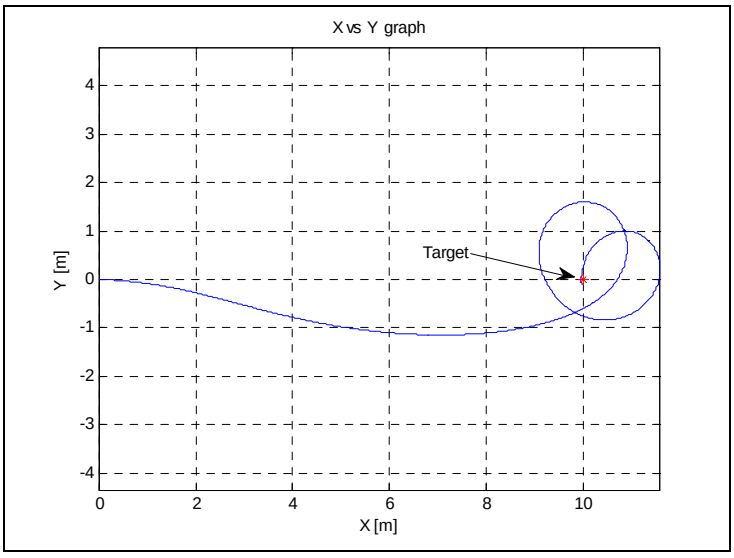

Figure 28 Vehicle Motion in X-Y plane

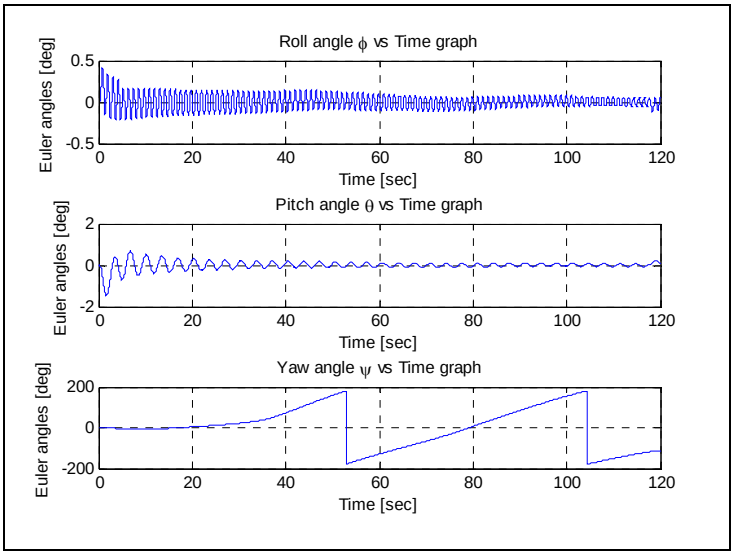

Figure 29 Euler Angles of the vehicle

Due to the drag force of the current, the vehicle experiences a side slip. Since the autopilot tries to keep the yaw angle on the line of sight of the target, the vehicle starts to turn around to the target location. Because the control does not include the sway velocity, the sway motion caused by the current can not be compensated. Due to this lateral drift, it is very likely that the vehicle skips the target. In fact it is seen that it does so in Figure 29 in the first attempt.

4.5 Effect of Hydrostatic Restoring Moment

4.5.1 Position Control in the Presence of an Initial Roll Angle

As we described earlier in Chapter 3, the roll motion of the vehicle is not directly controlled by any of the thruster. The roll stability can be maintained only by the hydrostatic restoring moment. To test the effectiveness of this restoring moment, we

give an initial roll angle ($\phi_0 = 45^0$) to the vehicle. The commended position is the origin of the earth fixed reference frame. That is:.

$$\bar{x}_c = \begin{bmatrix} u_c & w_c & q_c & x_c & y_c & z_c & \theta_c \end{bmatrix}^T = \begin{bmatrix} 0 & 0 & 0 & 0 & 0 & 0 & 0 \end{bmatrix}^T \quad (3.9)$$

The response to this disturbance is shown in Figure 30 and Figure 31:

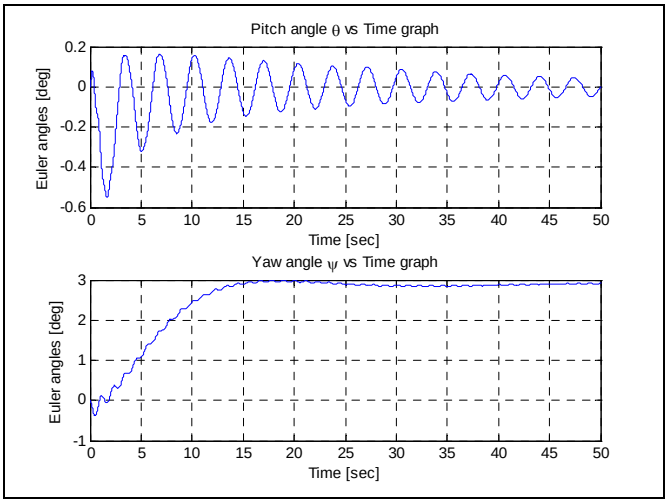

Figure 30 Vehicle Euler Angles

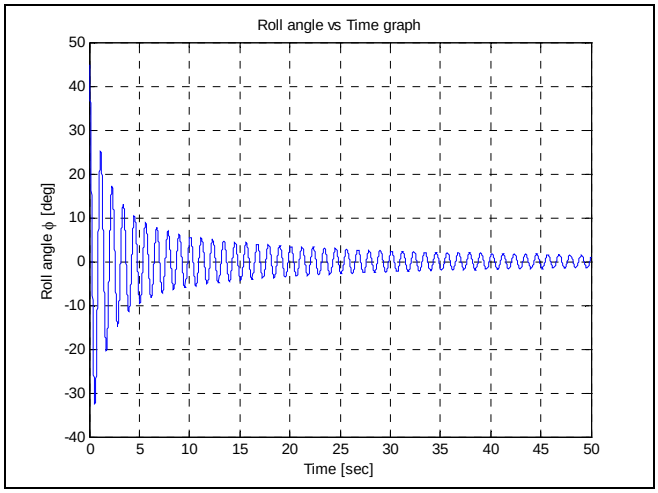

Figure 31 Roll angle

Naturally, the system oscillates in this case and due to the roll damping effect of the surrounding water, the magnitude of the oscillations decreases. The resulting variations of the earth frame coordinates of the vehicle are depicted in Figure 32.

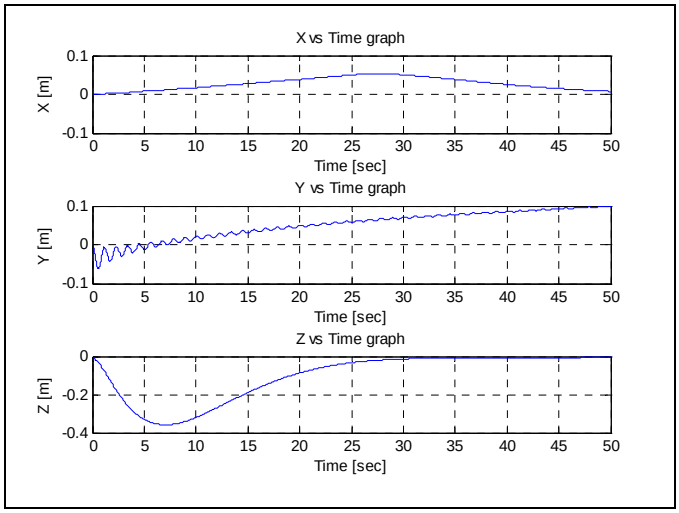

Figure 32 Vehicle Positions

As seen in the *z* plot of Figure 32 the vehicle initially ascends. This is because the initially non-zero roll angle reduces the vertical component of the commanded thrust force by the depth controller which is designed with the assumption of zero roll angle. Meanwhile, again due to the non-zero roll angle, the horizontal component of the commanded thrust force causes the vehicle to move in the *y* axis of the earth fixed frame as seen in the *y* plot of Figure 32. However, due to the combined effect of hydrostatic restoring and hydrodynamic damping moments, the roll angle reduces to zero after a while. Hence the commanded thrust force is used fully to correct the depth error. At the same time the lateral component of the thrust force disappears and thus the motion in *y* direction stops.

4.5.2 Position Control in the Presence of an Initial Roll and Pitch Angle

To further test the robustness of the system we gave initial pitch and roll angle to the system ($\theta_0 = 45^0, \phi_0 = 45^0$) and commanded a tight turn to change its position to

locate itself at the earth fixed coordinates ($[x_e, y_e] = [0,10]$). This motion requirement is specified as:

$$\bar{x}_c = [u_c \quad w_c \quad q_c \quad x_c \quad y_c \quad z_c \quad \theta_c]^T = [0 \quad 0 \quad 0 \quad 0 \quad 10 \quad 0 \quad 0]^T \quad (3.10)$$

The responses of the system are shown in Figure 33and Figure 34:

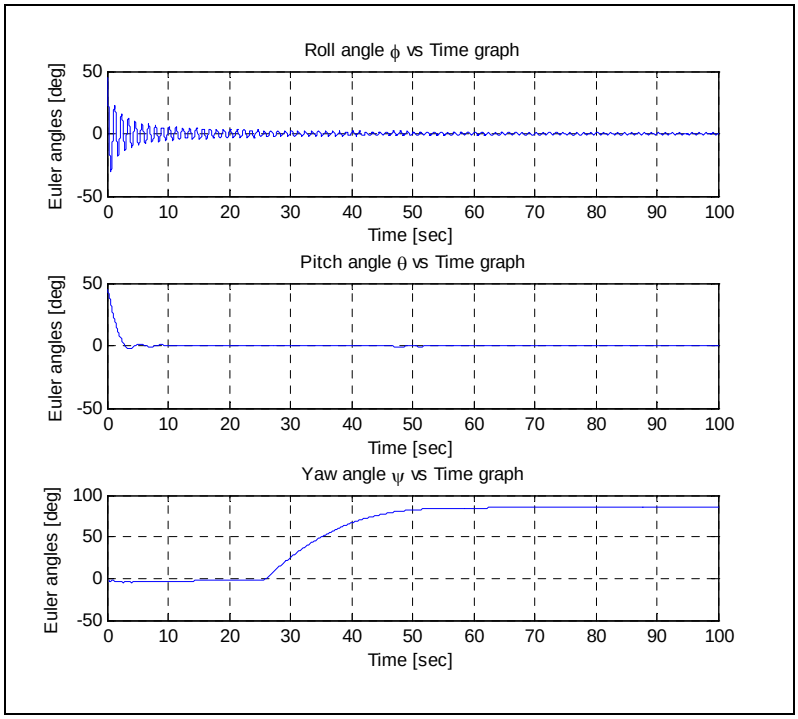

Figure 33 Euler Angles of vehicle

Since the vehicle has a active control in the pitch motion, attenuation in the pitch angle is much faster than the roll angle:

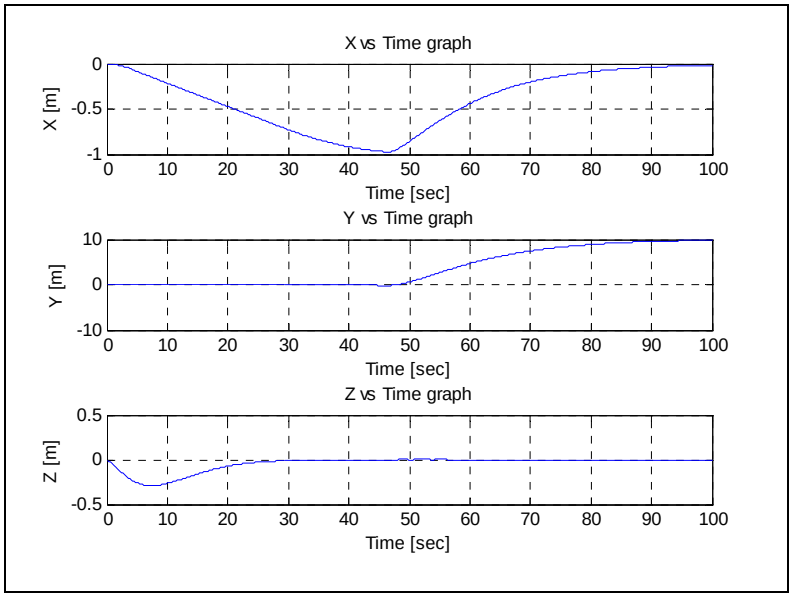

Figure 34 Positions of the vehicle

As we stated above due to the positive buoyancy of the vehicle, depth controllers commanded to the aft-front thrusters a net positive thrust. The positive pitch angle changed the alignment of the net thrust to be in the negative *x* direction of the earth fixed frame. Since the port and the starboard thrusters halted by the autopilot for 25 seconds to wait for the attenuation of the roll angle, the vehicle slips through the negative *x* direction. Following the stabilization of the roll angle, the position controllers of the vehicle achieved to reach the desired position.

4.5.3 Effects of Added Dead Weight

Since the center of gravity can be transferred by adding a dead weight, the effect of the relocated center of gravity on the system response has to be investigated. The results of the response of the vehicle to an initial roll angle ($\phi_0 = 45^0$) is shown in Figure 35. A lumped mass of 5 kg is located half meters below the origin of the

body fixed frame. Afterward, position of the transported center of gravity and the inertia dyadic is recalculated. The desired position of the vehicle is specified as:

$$\bar{x}_c = \begin{bmatrix} u_c & w_c & q_c & x_c & y_c & z_c & \theta_c \end{bmatrix}^T = \begin{bmatrix} 0 & 0 & 0 & 0 & 0 & 0 & 0 \end{bmatrix}^T \quad (3.11)$$

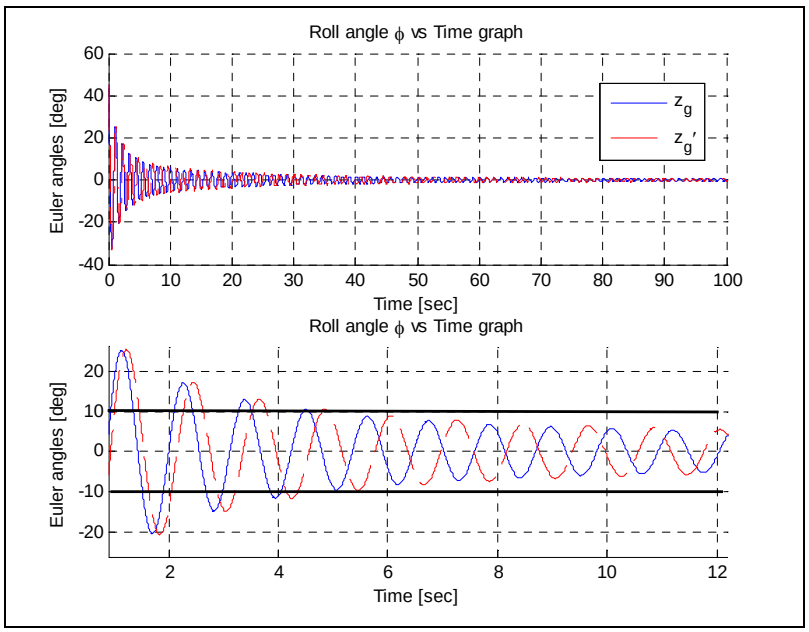

Figure 35 Roll angles for different z_g

It can be seen that the increase in the distance of the center of gravity results in a decrease in the amplitude and the frequency of the roll angle oscillations.

CHAPTER 5

CONCLUSION AND FUTURE WORK

5.1 Conclusion

In this research the physical phenomena behind the motion of an underwater vehicle is tried to be modeled. The vehicle is modeled as a rigid body. The non-linearity effects are included in modeling the hydrodynamic forces and moments. Furthermore the thrusters are modeled as realistically as possible considering the interaction of the surrounding water with the blades, the electrical motor characteristics and the motor drivers.

Another objective of this work is to design position and rate controllers. As it is stated, the underwater vehicle dynamics are non-linear and coupled. Therefore we linearize the dynamics about certain selected reference motions which are used to constitute the basis of possible maneuvers. These basic motions are selected as the surge, heave/pitch and yaw motions.

Design of the controllers for the basic motions is based on the state feedback methodology. We found the feedback gains by means of linear quadratic regulator optimization. Energy consumption is a key requirement for UUV design due to the limited energy storage on board. That is why optimal control is used, rather than classical control methods.

On top of these basic motion controllers, an autopilot is developed to manage the combination of basic motions for a desired maneuver. This autopilot improves the over all control effectiveness by posing due limitations on the thrusters to prevent the excessive power consumption.

We tested these controllers and the autopilot with the simulation tool developed which employs the complete nonlinear dynamics. The simulation module was developed to be a generic tool, which can be used for other types of underwater vehicles as well.

The vehicle performance is tested for typical maneuvers. The results of the simulations showed that the performance of the designed controllers is capable of making the maneuvers quiet satisfactorily.

The chosen vehicle configuration is an under actuated system because the onboard thrusters can control only four of the six degrees of freedom. The fifth degree of freedom which is the roll motion is stabilized by the hydrostatic restoring and hydrodynamic damping moments. However the sixth degree of freedom, which is the sway motion, can not be controlled at all.

Te effect of the length of the hydrostatic moment arm on the roll stability of the vehicle is particularly examined. In this examination, a lumped mass is virtually added under the center of gravity with at different positions to increase the magnitude of the moment arm. As we expected, oscillations the roll angle are reduced in magnitude and frequency. Therefore the roll stability is improved.

In another test case, we investigated the effect of the underwater currents on the sway motion of the vehicle. If the vehicle encounters to a lateral current, the vehicle experiences a lateral drift, because none of the onboard thrusters is aligned in the sway direction. However this lateral drift can be indirectly controlled to some extend, with appropriate sequential manipulations of the surge and yaw controllers by the autopilot.

We also examined the torque effect of the thrusters occurred as a result of fluid interference with the propeller rotation. The simulation results are presented in Appendix B. The conclusions are examined for different configurations of blade angle and with different maneuvers which means different rotation directions.

It can be concluded that the pitch angle of the propeller blade angles for the port and the starboard thrusters can be chosen by the help of maneuver specifications. If the vehicle mission needs tight turns the propeller pitch angles have to be the same to prevent the roll angle during turns. On the other hand, if the vehicle is commanded to travel long distances in the surge control mode and turns are needed very rare, it is better to choose the propeller angles twisted. For the aft and the front thrusters, the decision to change the blade pitch angles is straightforward, since the reversed pitch angle improves the motion effectiveness. Because the vehicle is positively buoyant, vertical plane thrusters are continuously working. Therefore a continuous yaw moment disturbance is applied to the vehicle if the propellers are identical.

5.2 Future work

This study covers the base approach for a motion control of an underwater vehicle. The designed controllers are lack of disturbance rejection feature. So as a future work some disturbance models can be added to the simulation tool. Some of disturbance model which may be needed to accomplish the desired operational effectiveness are surface wave models, an advance hydrodynamic model which includes ground effects, effects of the wake formed due to thrusters, turbulence models and more complex current models.

In this work it is assumed that all sensors are perfect and have no noise, bias or error on the output. Furthermore, readings from the states assumed to be taken in the continuous time. So for a further study, effects of digitization can be investigated.

Another issue that may be added on to this work is designing observers to predict the states. We assume all states are observable but real life problems may lead to missed measurements. These observers also may be used to handle hydrodynamic data so the systems response may be proceed since controller errors due to faulty coefficients by means of manipulation of controller gains.

On this thesis three motion controllers are designed, which use three separated linearization points. It may be a good further work to combine these linearization points and model the system into one state space representation. By achieving this, one can succeed to apply full state feedback controllers and accomplish to make the vehicle move in advance maneuvers.

Another useful future addition may be developing a more advanced autopilot including adaptive and decisive features.

REFERENCES

1 Christopher D. Chuhran, *"Obstacle Avoidance Control For The Remus Autonomous Underwater Vehicle"* September 2003 Naval Post graduate School.

2 Douglas L. Williams *"Loitering Behavior Of Autonomous Underwater Vehicles"* June 2002 Naval Postgraduate School.

3 Timothy Prestero *"Verification of a Six-Degree of Freedom Simulation Model for the REMUS Autonomous Underwater Vehicle"* Massachusetts Institute Of Technology and the Woods Hole Oceanographic Institution September 2001

4 J. Yuh, Jing Nie, and C.S.G. Lee *"Experimental Study on Adaptive Control of Underwater Robots"* Proceedings of the 1999 IEEE International Conference on Robotics & Automation Detroit, Michigan May 1999

5 Gianluca Antonelli, Stefano Chiaverini, Nilanjan Sarkar, and Michael West *"Adaptive Control of an Autonomous Underwater Vehicle: Experimental Results on ODIN"* IEEE Transactions On Control Systems Technology, vol. 9, no. 5, september 2001

6 Joseph J. Keller *"Tracking Control Of Autonomous Underwater Vehicles"* December 2002 Naval Postgraduate School

7 Lingli Ni *"Fault-Tolerant Control of Unmanned Underwater Vehicles"* Virginia Polytechnic Institute and State University June 29, 2001.

8 Andrea Senani, Silvia M. Zanoli *"Designing, guidance and control schemes for UUVs using an integrated simulation environment"* Proceedings of the 1998 IEEE International Conference on Control Applications Trieste, Italy 1-4 September 1998

9 A.J. Healey, F.A. Papoupol, R. Cristi *"Design and Experimental verification of a model based compensator for rapid UUV depth control"*

10 Anthony J. Healey and David Lienard *"Multivariable Sliding Mode Control for Autonomous Diving and Steering of Unmanned Underwater Vehicles"* IEEE Journal Of Oceanic Engineering, vol. 18, no. 3, july 1993

11 A. J. Healey, S. M. Rock, S. Cody, D. Miles, and J. P. Brown *"Toward an Improved Understanding of Thruster Dynamics for Underwater Vehicles"* IEEE Journal Of Oceanıc Engıneerıng, VOL. 20, NO. 4, October 1995

12 Håvard Bø *"Hydrodynamic Estimation AND Identification"* Norwegian University of Science and Technology, NTNU Department of Engineering Cybernetics Trondheim, Norway 2nd August 2004

13 T. I. Fossen *"Guidance and Control of Ocean Vehicles"* John Willey& Sons

14 Bernard Etkin, Lloyd Duff Reid, "*Dynamics of flight Stability and Control 3rd edition"* pg. 313

15 Gray, Edwyn "*The Devil's Device – Robert Whitehead and the History of the Torpedo*." Annapolis, Maryland: Naval Institute Pres 1991

16 J. N. Newman. *"Marine Hydrodynamics"* MIT Press, Massachusetts, 1977.

17 J. Yuh *"Learning Control for Underwater Robotic Vehicles"* IEEE Transactions On Control Systems Technology 1994

18 Dana r. Yoerger, Jean-Jacques e. Slotine *"Robust Trajectory Control of Underwater Vehicles"* IEEE Journal Of Oceanic Engineering, vol. oe-10, no. 4, October 1985

19 Wan-Chung LAM, Tamaki URA *"Non-Linear Controller with Switched Control Law for Tracking Control of Non-Cruising AUV"* IEEE Journal Of Oceanic Engineering, 1996

20 Andrea Senani, Silvia M. Zanoli *"Designing, guidance and control schemes for AUVs using an integrated simulation environment"* Proceedings of the 1998 IEEE International Conference on Control Applications

21 Robert D. Blevins. "*Formulas for Natural Frequency and Mode Shape"*, Kreiger Publishing, Florida, 1979.

APPENDIX A

SIMULATION OVERVIEW

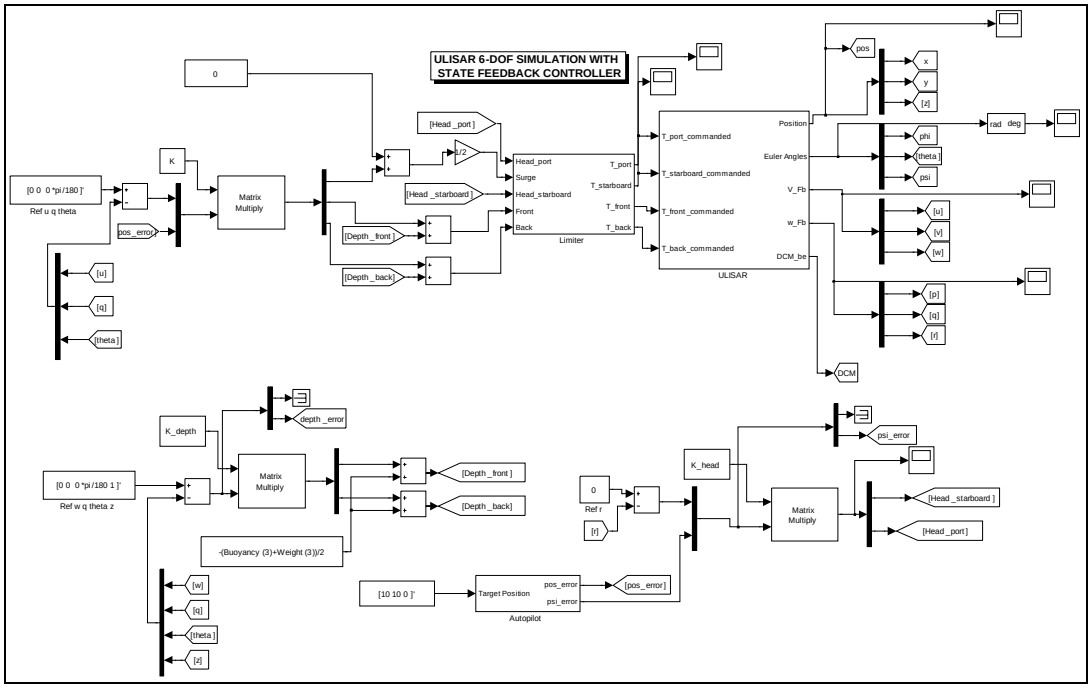

Figure 36 General View of Simulation

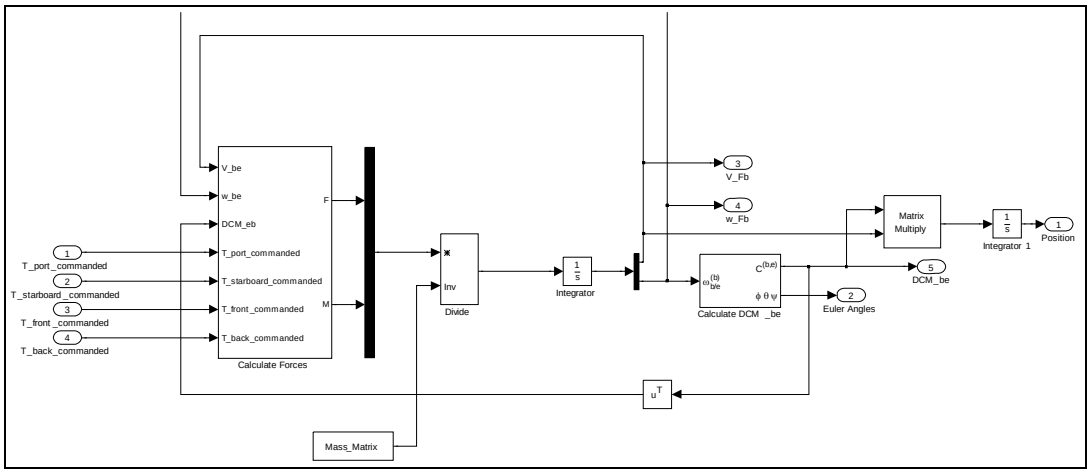

Figure 37 Equation of Motion Calculation

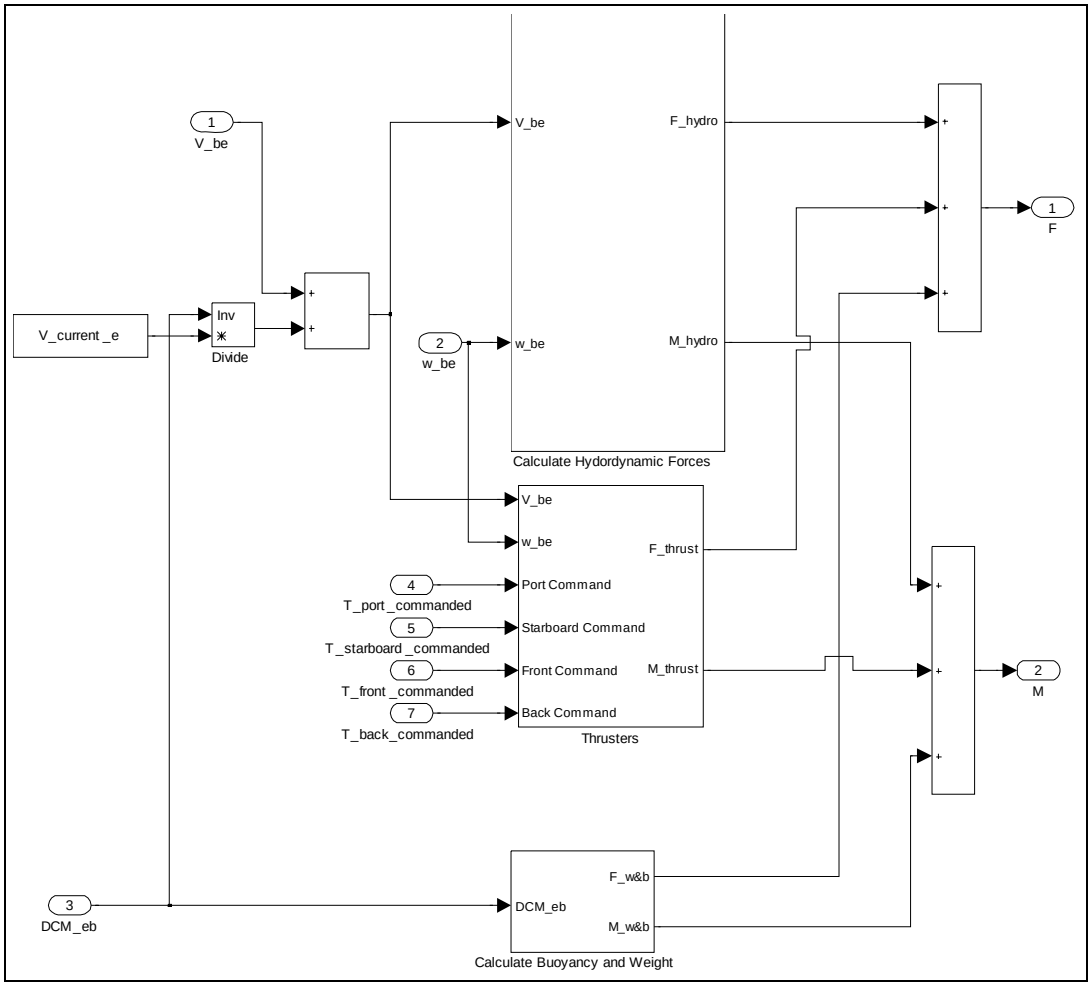

Figure 38 Calculate Forces

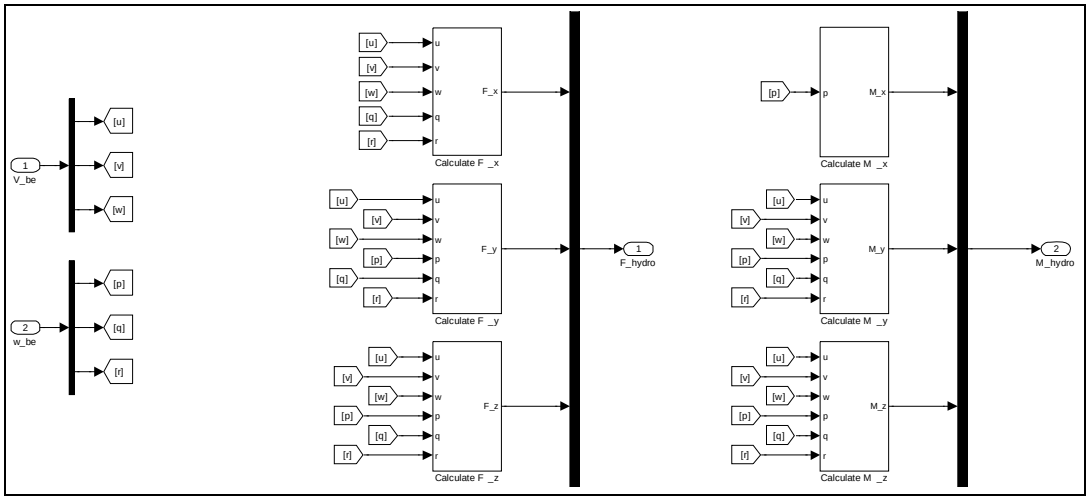

Figure 39 Calculate Hydrodynamic Forces

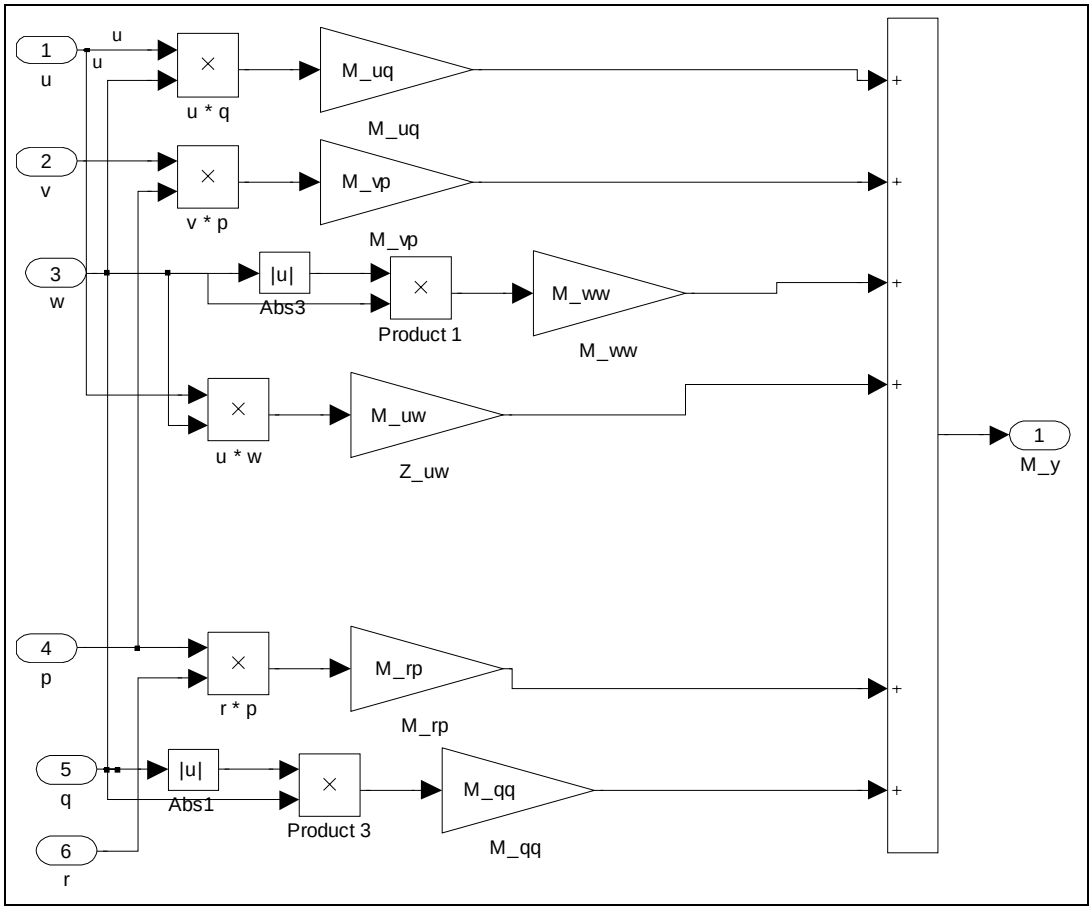

Figure 40 Sample hydrodynamic force calculation

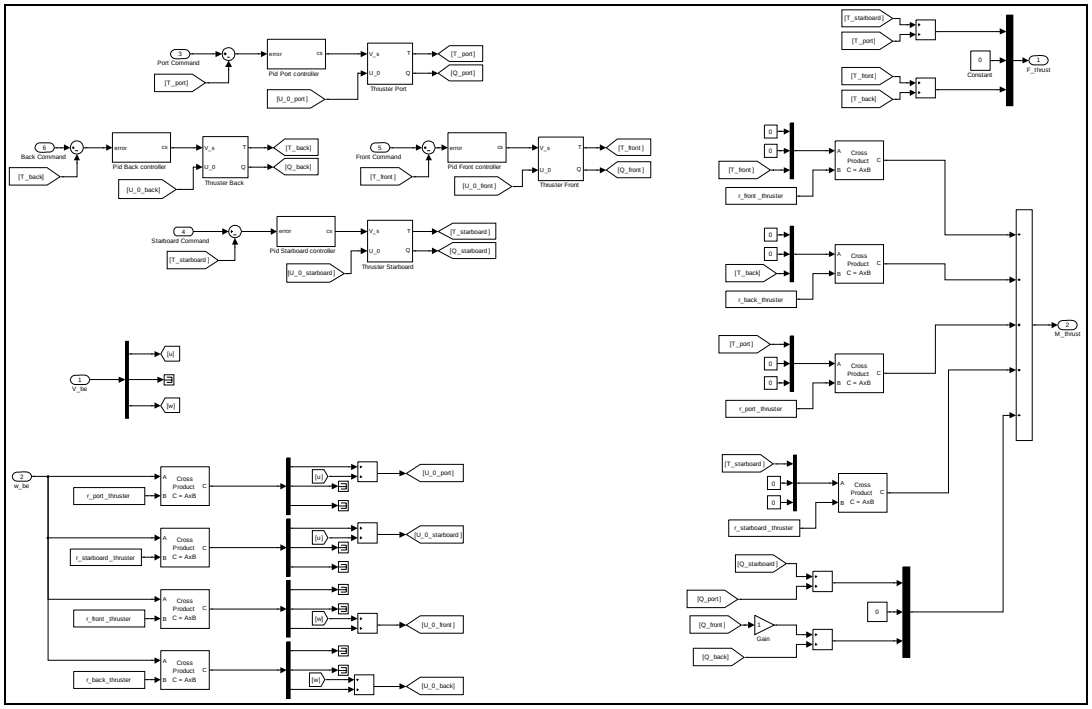

Figure 41 Calculate Thruster Forces and Moments

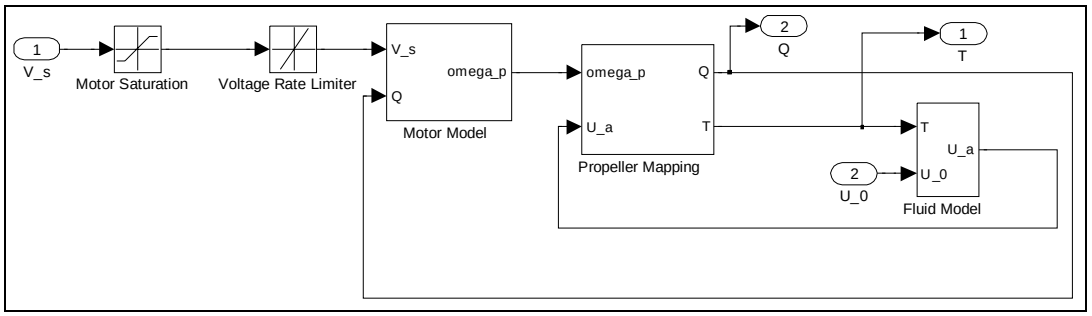

Figure 42 Thruster Model

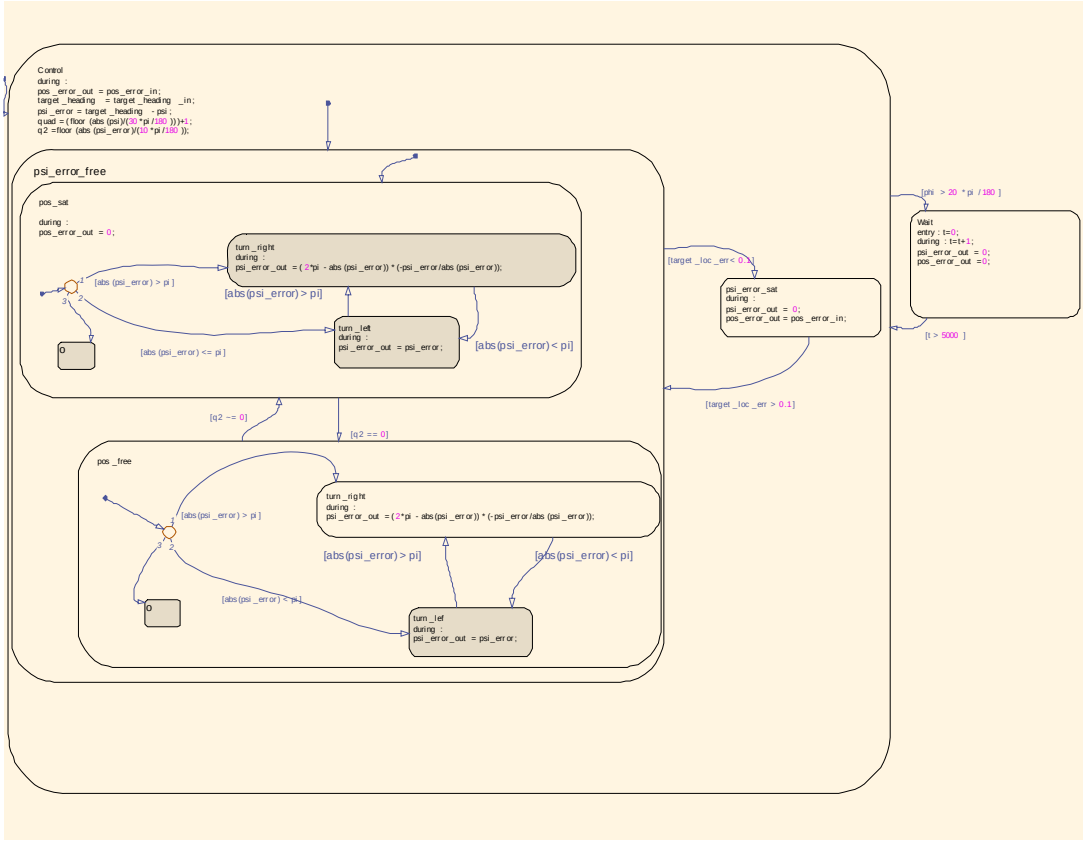

Figure 43 Autopilot

APPENDIX B

THRUSTER BLADE ANGLE

The pitch angle of the propeller effects the vehicle is depend on the maneuver the vehicle made. Therefore we can group the results as given below:

1. Port – Starboard thrusters:

    a. Same blade pitch angle:

        i. In surge motion the moments produced by thrusters adds on causes roll angle

        ii. In tight turns as we described earlier we make the vehicle wait until desired heading angle accomplished. So the net torque produced by the difference which result in small torque and small roll angle

        iii. During surge and heading controllers work simultaneously the resultant torque on roll axis is found between the above two situations with a tendency of a increasing roll angle.

    b. Reversed blade pitch angle:

        i. In surge motion the moments produced by subtracted from each other thus net torque is nearly zero resulting small roll angle.

        ii. In tight turns the net torque can be found by adding torques of two thrusters on top of each other. This causes a roll angle furthermore combined with the rotational effects of turning dynamics decreases control efficiency.

iii. When surge and heading controllers work simultaneously the resultant torque on roll axis is smaller compared to a turn only maneuver case.

2. Front – Aft thrusters:

Since vehicle is positively buoyant vertical plane thrusters are continuously working. Therefore the effect of their rotational torque is much more significant. In addition, due to big pitch damping on vehicle and need of setting pitch angle to zero, the requirement for use of these controllers in opposite direction to create pitch moment is fewer than the need of horizontal controllers to make turns. The results based on configuration is given below

a. Same blade pitch angle configuration: During vehicle try to sustain its depth, vertical thrusters produce a net yaw torque and a heading error occurs. In chain reaction yaw controllers start to work and vehicle start to oscillates around a desired yaw.

b. Reversed blade pitch angle: Since the torque direction is different when the depth control mode is active the net torque produced by this configuration is very small. Therefore it is a good alternative for original configuration.

1. Port-Starboard Blade Pitch Angles Twisted:

a. Tight turn:

$$\bar{x}_c = \begin{bmatrix} u_c & w_c & q_c & x_c & z_c & \theta_c \end{bmatrix}^T = \begin{bmatrix} 0 & 0 & 0 & 1 & 10 & 0 \end{bmatrix}^T$$

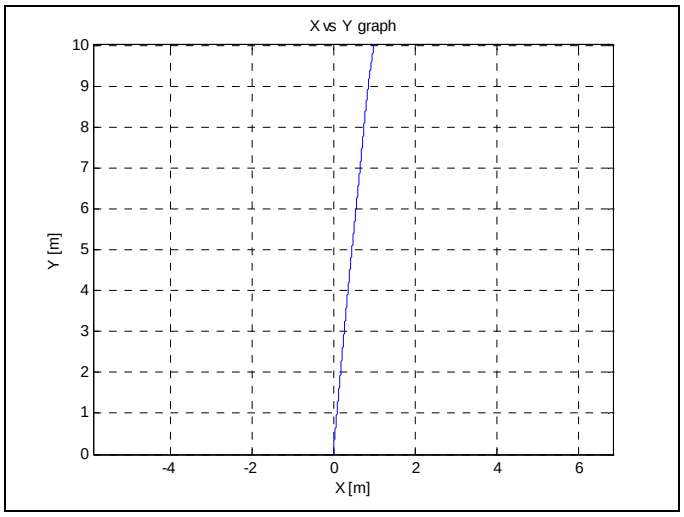

Figure 44 Position plot

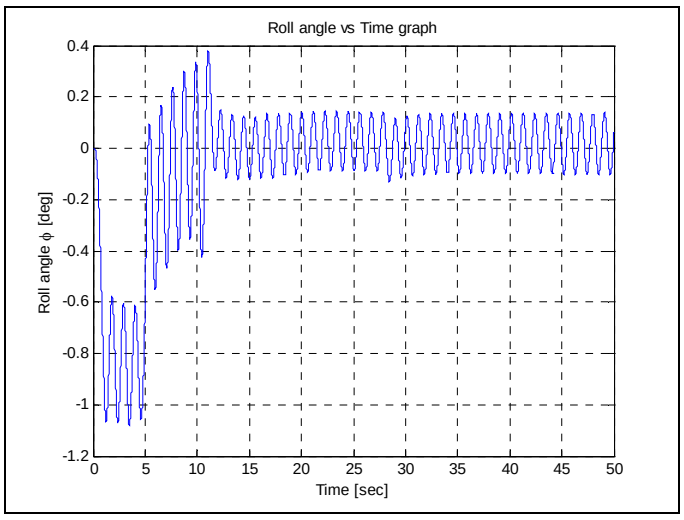

Figure 45 Roll angle of the vehicle

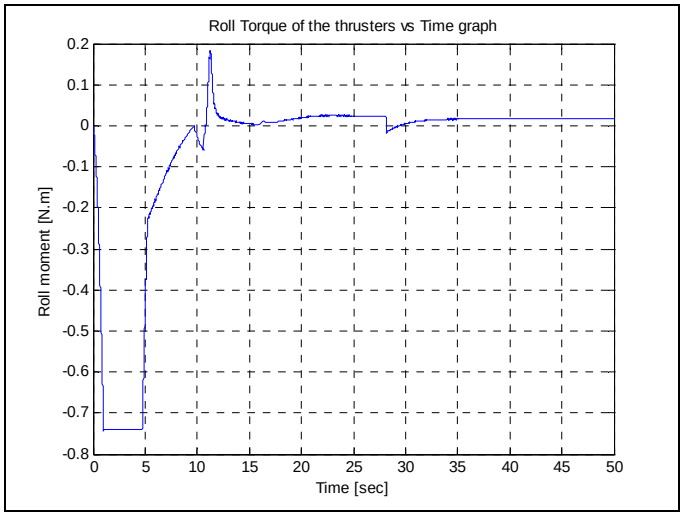

Figure 46 Roll torque applied by thrusters

b. Forward Motion:

$$\bar{x}_c = \begin{bmatrix} u_c & w_c & q_c & x_c & z_c & \theta_c \end{bmatrix}^T = \begin{bmatrix} 0 & 0 & 0 & 20 & 0 & 0 \end{bmatrix}^T$$

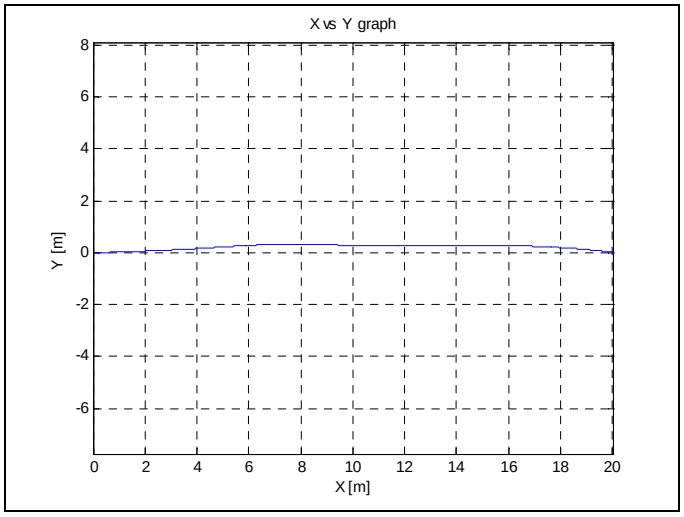

Figure 47 Position plot

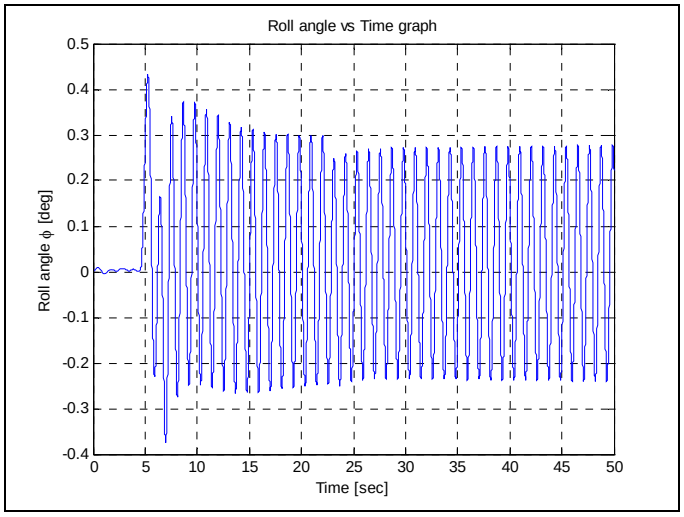

Figure 48 Roll angle of the vehicle

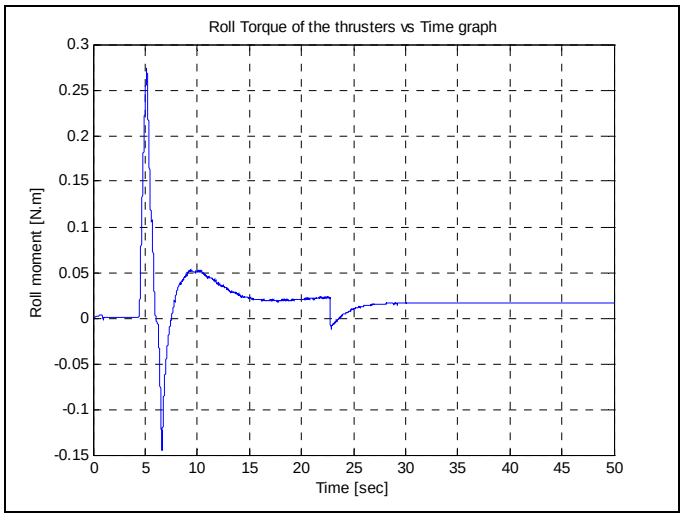

Figure 49 Roll torque applied by thrusters

2. Front-aft Blade Pitch Angles Twisted:

a. Tight turn:

$$\bar{x}_c = \begin{bmatrix} u_c & w_c & q_c & x_c & z_c & \theta_c \end{bmatrix}^T = \begin{bmatrix} 0 & 0 & 0 & 1 & 10 & 0 \end{bmatrix}^T$$

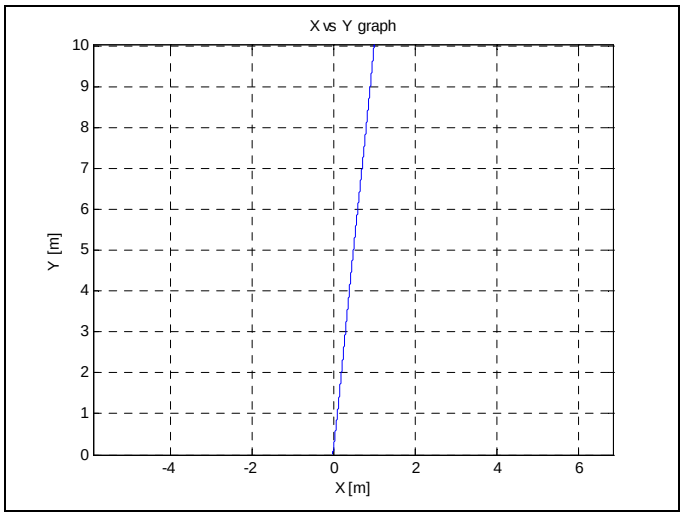

Figure 50 Position plot

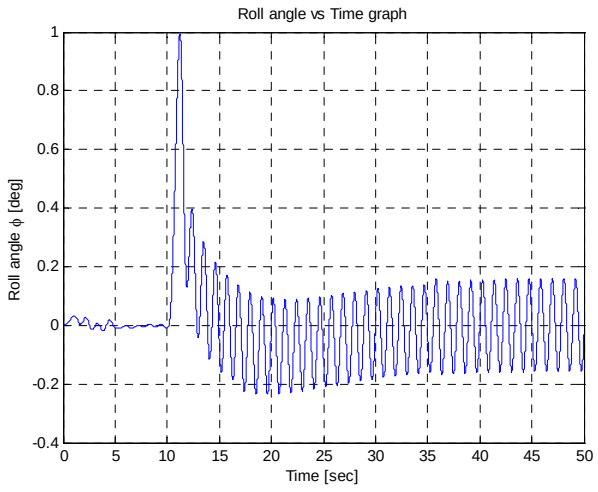

Figure 51 Roll angle of the vehicle

b. Forward Motion:

$$\bar{x}_c = \begin{bmatrix} u_c & w_c & q_c & x_c & z_c & \theta_c \end{bmatrix}^T = \begin{bmatrix} 0 & 0 & 0 & 20 & 0 & 0 \end{bmatrix}^T$$

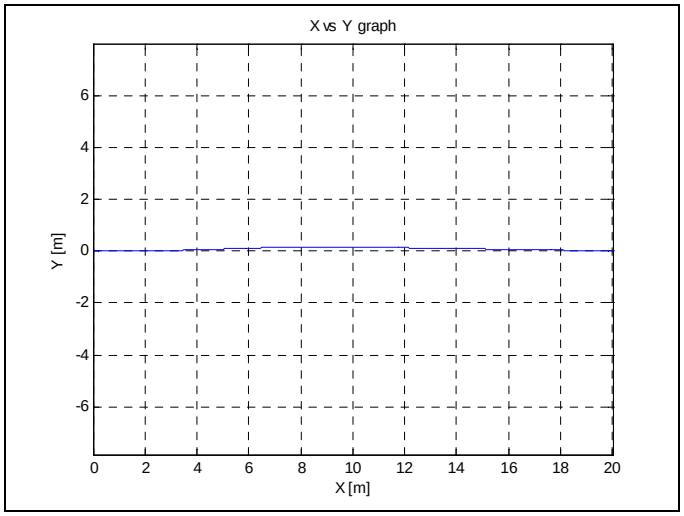

Figure 52 Position plot

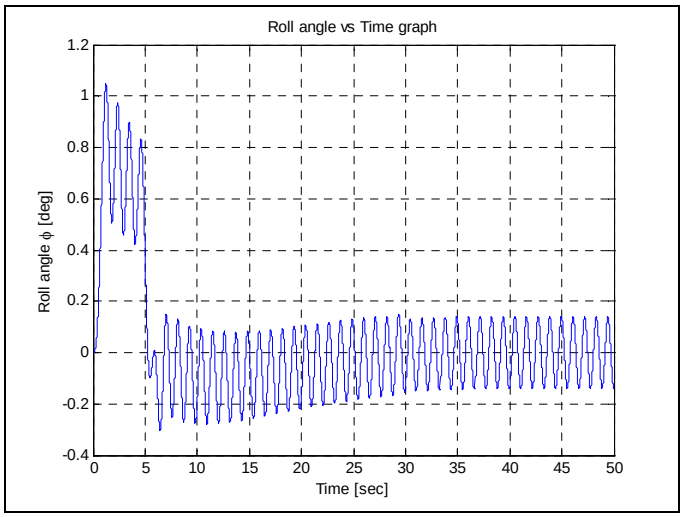

Figure 53 Roll angle of the vehicle

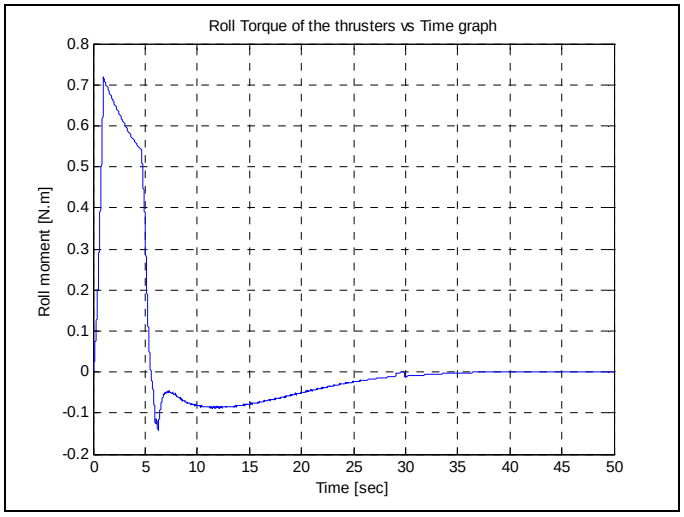

Figure 54 Roll torque applied by thrusters

3. Blades Pitch Angles Front-aft and Port-Starboard Thrusters Twisted:

a. Tight turn:

$$\bar{x}_c = \begin{bmatrix} u_c & w_c & q_c & x_c & z_c & \theta_c \end{bmatrix}^T = \begin{bmatrix} 0 & 0 & 0 & 1 & 10 & 0 \end{bmatrix}^T$$

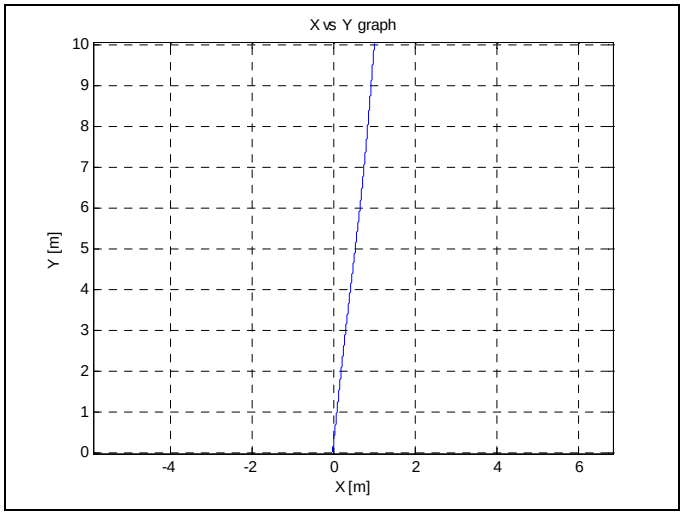

Figure 55 Position plot

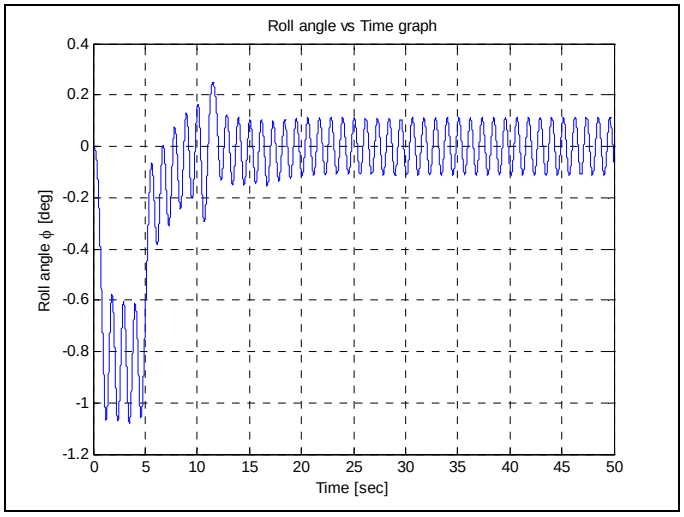

Figure 56 Roll angle of the vehicle

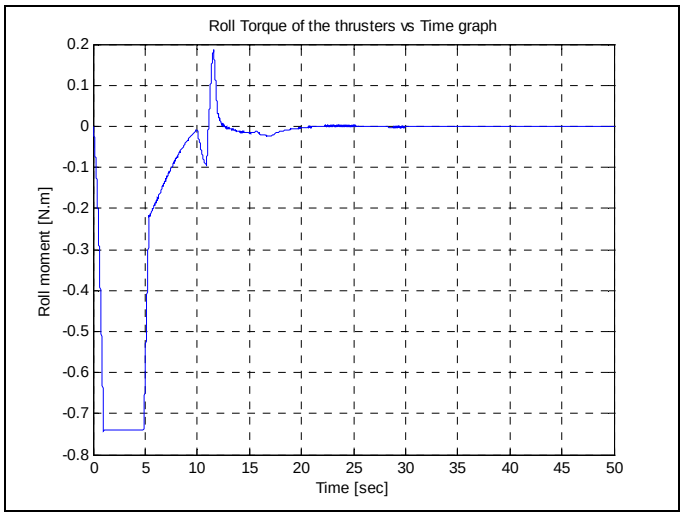

Figure 57 Roll torque applied by thrusters

b. Forward Motion:

$$\bar{x}_c = \begin{bmatrix} u_c & w_c & q_c & x_c & z_c & \theta_c \end{bmatrix}^T = \begin{bmatrix} 0 & 0 & 0 & 20 & 0 & 0 \end{bmatrix}^T$$

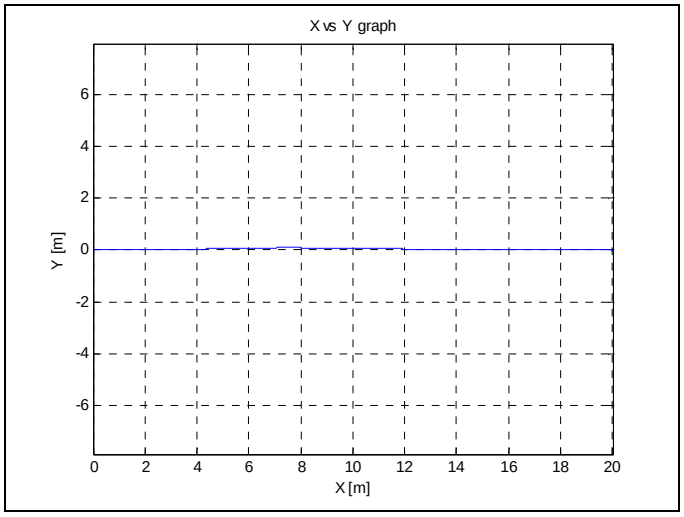

Figure 58 Position plot

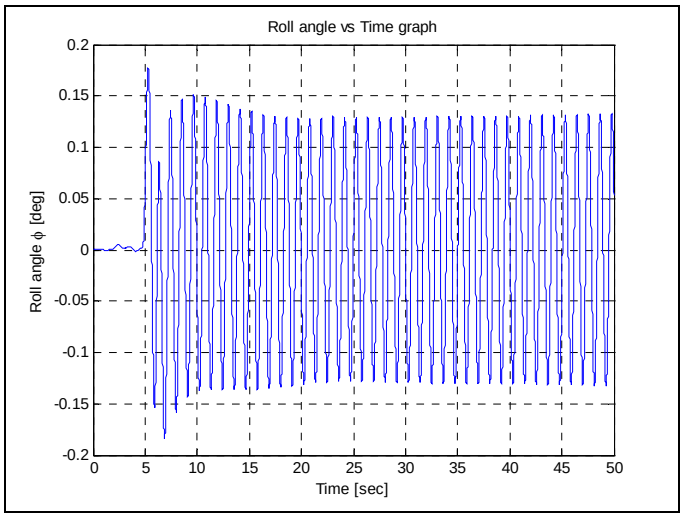

Figure 59 Roll angle of the vehicle

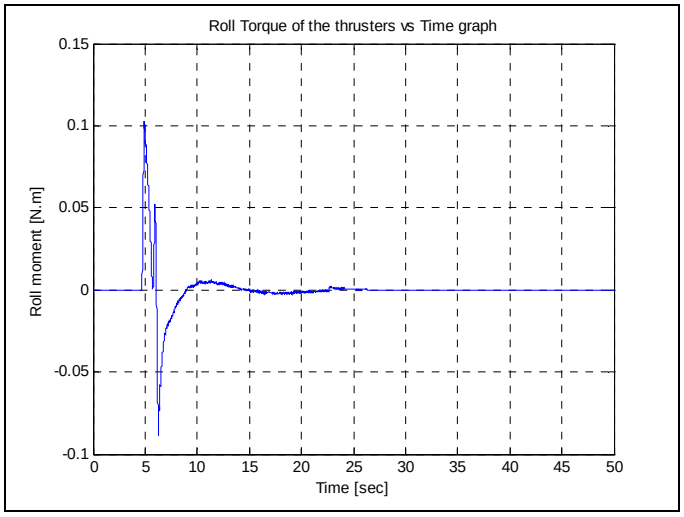

Figure 60 Roll torque applied by thrusters

APPENDIX C

HYDRODYNAMIC DATA

Table 7 Body Reference Frame x_b axis Hydrodynamic Force Coefficients

Parameter	Value	Units
$X_{\dot{u}}$	-1.3586	kg
$X_{u\|u\|}$	-9.5426	kg/m
X_{wq}	-131.5006	kg/rad
X_{qq}	-24.4317	kg m/rad
X_{vr}	131.5006	kg/rad
X_{rr}	-24.4317	kg m/rad

Table 8 Body Reference Frame y_b axis Hydrodynamic Force Coefficients

Parameter	Value	Units
$Y_{\dot{v}}$	-131.5006	kg
$Y_{\dot{r}}$	24.4317	kg/rad
$Y_{v\|v\|}$	-258.7976	kg/m
$Y_{r\|r\|}$	14.472	kg m /rad^2
Y_{ur}	23.3523	kg m/rad
Y_{wp}	131.5006	kg/rad
Y_{pq}	24.4317	kg m/rad
Y_{uv}	-71.2397	kg/m

Table 9 Body Reference Frame z_b axis Hydrodynamic Force Coefficients

Parameter	Value	Units
$Z_{\dot{w}}$	-131.5006	kg
$Z_{\dot{q}}$	-24.4317	kg/rad
$Z_{w\|w\|}$	-258.7976	kg/m
$Z_{q\|q\|}$	-14.472	kg m /rad^2

Table 9 (continued) Body Reference Frame z_b axis Hydrodynamic Force Coefficients

Parameter	Value	Units
Z_{uq}	-23.3523	kg m/rad
Z_{vp}	-131.5006	kg/rad
Z_{rp}	24.4317	kg m/rad
Z_{uw}	-71.2397	kg/m

Table 10 Body Reference Frame x_b axis Hydrodynamic Moment Coefficients

Parameter	Value	Units
$K_{\dot{p}}$	-0.13	kg m^2/rad
$K_{p\|p\|}$	-0.3922	kg m^2/rad^2

Table 11 Body Reference Frame y_b axis Hydrodynamic Moment Coefficients

Parameter	Value	Units
$M_{\dot{w}}$	-24.4317	kg m
$M_{\dot{q}}$	-4.7837	kg m^2/rad^2
$M_{w\|w\|}$	16.1602	kg
$M_{q\|q\|}$	-13.96	kg m^2/rad^2
M_{uq}	4.0685	kg m/rad
M_{vp}	-24.4317	kg m/rad
M_{rp}	4.3915	kg m^2/rad^2
M_{uw}	-115.3319	kg

Table 12 Body Reference Frame z_b axis Hydrodynamic Moment Coefficients

Parameter	Value	Units
$N_{\dot{v}}$	-24.4317	kg m
$N_{\dot{r}}$	-4.7837	kg m^2/rad^2
$N_{v\|v\|}$	-16.1602	kg
$N_{r\|r\|}$	-13.96	kg m^2/rad^2
N_{ur}	4.0685	kg m/rad
N_{wp}	-24.4317	kg m/rad
N_{pq}	-4.3915	kg m^2/rad^2
N_{uv}	-95.5305	kg